



## Anton de Kom Universiteit van Suriname

Faculteit der Technologische Wetenschappen  
Studierichting Werktuigbouwkunde

STUDIERICHTING  
WERTUIGBOUWKUNDE

**Wb**



---

### Experimental and Numerical Study of the Performance Characteristics of a Pico Hydro Turbine Manufactured by Indalma Industries Inc.

---

**Students:**

Ramsay Mac Donald 09WB1018  
Nigel Sloot 09WB1030

**Supervisor:**

dr. ir. Nawin Ryan Nannan

**Co-Supervisor:**

dr. Rudi Henri van Els

Date:

May 9<sup>th</sup> 2014



Kennis maken en kennis delen in duurzaam partnerschap

---

**Ramsay Mac Donald 09WB1018**

**Nigel Sloot 09WB1030**

*Experimental and Numerical Study of the Performance Characteristics of a Pico Hydro Turbine Manufactured by Indalma Industries Inc.*

Paramaribo, May 9<sup>th</sup> 2014

Reviewers: ir. Jimmy Narain and Amrish Daniel Lachman, PhD CMRP

Supervisors: dr. ir. Nawin Ryan Nannan and dr. Rudi Henri van Els

**Anton de Kom University of Suriname - AdeKUS**

Faculty of Technology - FTeW

Mechanical Engineering Discipline

Keywords: CFD, Indalma turbine, Performance characteristics, Pico hydropower.

---

**Report Number:23NRN14**

Anton de Kom University of Suriname - AdeKUS



Faculty of Technology - FTeW  
Mechanical Engineering Discipline

## **Experimental and Numerical Study of the Performance Characteristics of a Pico Hydro Turbine Manufactured by Indalma Industries Inc.**

Report submitted for the conclusion of the Mechanical Engineering course at the Anton de Kom University of Suriname, as a partial requirement for obtaining title Bachelor of science in Mechanical Engineering.

Ramsay Mac Donald 09WB1018  
Nigel Sloot 09WB1030

*1. Reviewer*      ir. Jimmy Narain  
Mechanical Engineering Discipline  
Anton de Kom University of Suriname - AdeKUS

*2. Reviewer*      Amrish Daniel Lachman, PhD CMRP  
Mechanical Engineering Discipline  
Anton de Kom University of Suriname - AdeKUS

*Supervisors*      dr. ir. Nawin Ryan Nannan and dr. Rudi Henri van Els

May 9<sup>th</sup> 2014



*This work is dedicated to adult children  
who dreamt of becoming scientists when they were little.*



# Acknowledgement

We gratefully acknowledge the contributions of the Mechanical Engineering Discipline (WB) of the Anton de Kom University of Suriname (AdeKUS) and the University of Brasilia (UnB) in funding the project of which this report is part of.

This report would not have been possible without the inspiration and support of our supervisors Nawin Ryan Nannan and Rudi Henry van Els.

Our thanks and appreciation go to all of the wonderful individuals who were part of this journey such as the faculty members who supported us: Jimmy Narain, Daniel Lachman, Sieuwnath Naipal, Cyrano Vasseur, Samuel Karjiodjiwongso, Robert Mungro Anand Kalpoe and Clint Ally, a special contributor: Jan Kaptein, and our project-colleagues at UnB: Olga Lucia, Rodrigo Calxita, Danilo Oliveira, Maria Carvalho and João Barreto.

Finally, we are eternally grateful to our friends and loved ones who supported us not only with this report, but throughout our lives.



# Summary

This work documents the results of a test project conducted in 2013 spanning a period of six months at the University of Brasilia (UnB) in collaboration with the Anton de Kom University of Suriname (AdeKUS). The aim of said project was to firstly determine the performance characteristics of a pico hydro turbine manufactured by Indalma Industries Inc. (3I), a company based in Brazil. As a second objective, a computational fluid dynamics (CFD) analysis was done to qualitatively identify, as a first assessment, the regions of flow losses in the turbine, and the interaction of the stator-rotor transition region. The experimental campaign at UnB yielded the following results, viz. the performance characteristics of the turbine in terms of the power-, flow- and efficiency curves as a function of the rotational speed of the shaft, as well as the turbine's specific speed. Moreover, the experimental results provided the boundary conditions for the CFD analyses. Using the experimental results as a reference (point of departure), the numerical analyses showed that due to the absence of inlet guide vanes (IGV), high (unquantified) losses occur within the stator-rotor transition region. Furthermore, given the fact that for this specific turbine, approximately midway the shroud, it is non-smooth and additionally exceeds the typical value of 15 degrees for the flow angle, extra, yet avoidable, losses are present.

**Keywords:** CFD, Indalma turbine, Performance characteristics, Pico hydropower.



# List of abbreviations and acronyms

<b>3I</b>	Indalma Industries Inc.
<b>AdeKUS</b>	Anton de Kom University of Suriname.
<b>BEP</b>	Best Efficiency Point.
<b>CFD</b>	Computational Fluid Mechanics.
<b>FGA</b>	Campus Gama of the UnB.
<b>IGV</b>	Inlet Guide Vanes.
<b>LE</b>	Leading Edge.
<b>PDAE</b>	Partial Differential and Algebraic Equation.
<b>SST</b>	Shear Stress Transport.
<b>TE</b>	Trailing Edge.
<b>UnB</b>	University of Brasilia.



## List of symbols

Symbols	Description	Unit
$E$	Euler's head	$\text{N} \cdot \text{m}^{-2}$
$f$	Frequency	Hz
$g$	Gravitational acceleration	$\text{m} \cdot \text{s}^{-2}$
$H$	Head at the turbine inlet	m
$n$	Rotational speed	rpm
$P$	Brake power at the turbine shaft	W
$\dot{Q}$	Water flow rate passing through the turbine rotor	$\text{m}^3 \cdot \text{s}^{-1}$
$\gamma$	Specific density of water	$\text{kN} \cdot \text{m}^{-3}$
$\rho$	Radial distance with respect to the axis of rotation	m
$\varphi$	Azimuth angle	deg
$\Omega$	Angular speed	$\text{rad} \cdot \text{s}^{-1}$
$\Omega_s$	Specific speed	rad

Subscripts	Description
min	Minimum
max	Maximum
*	Nominal



# Contents

<b>1</b>	<b>Introduction</b>	<b>1</b>
1.1	Introduction . . . . .	1
1.2	Problem definition & Objective . . . . .	2
1.3	Structure . . . . .	2
<b>I</b>	<b>Experimental Section</b>	<b>3</b>
<b>2</b>	<b>Brief Overview</b>	<b>5</b>
2.1	Hydro turbine classification . . . . .	5
2.2	Characteristics of hydro turbines . . . . .	6
2.2.1	Pelton Wheel . . . . .	7
2.2.2	Kaplan Turbine . . . . .	8
2.2.3	Francis Turbine . . . . .	9
2.3	Turbine control . . . . .	10
<b>3</b>	<b>Experimental Setup</b>	<b>13</b>
3.1	Commissioning of the test facility and design of experiment . . . . .	13
3.2	Instrumentation . . . . .	14
3.2.1	Flow- and Head-control . . . . .	14
3.2.2	De Prony brake . . . . .	15
3.2.3	Flow rate measuring instrument . . . . .	16
3.2.4	Pressure measuring instruments . . . . .	16
3.3	Data acquisition systems . . . . .	18
3.3.1	CW552 kit DAQ . . . . .	19
3.3.2	Arduino based DAQ . . . . .	19
3.3.3	Filtering the output data . . . . .	20
3.3.4	Response of the test facility . . . . .	21
3.4	Measurement procedure . . . . .	21
<b>4</b>	<b>Experimental Results &amp; Discussion</b>	<b>23</b>
4.1	Raw data . . . . .	23
4.2	Processed data & Discussion . . . . .	28
4.2.1	Submerged draft tube vs non-submerged draft tube . . . . .	28
4.2.2	Performance characteristics of the 3I turbine . . . . .	29

<b>II Numerical Analysis</b>	<b>35</b>
<b>5 Steady state numerical flow analysis of the pico hydro turbine under study at a single operating point</b>	<b>37</b>
5.0.3 Creating the Geometry . . . . .	38
5.0.4 Creating the Simulation Geometry . . . . .	39
5.0.5 Creating the Turbine Rotor in ANSYS BladeGen . . . . .	40
5.1 Creating the Rotor Mesh . . . . .	43
5.1.1 Meshing the Rotor Using TurboGrid . . . . .	43
5.1.2 Defining the Topology . . . . .	44
5.1.3 Reviewing the Mesh Data Settings . . . . .	44
5.1.4 Analyzing the Mesh . . . . .	44
5.2 Creating the Volute Mesh . . . . .	46
5.2.1 Generating the Octree Mesh . . . . .	46
5.2.2 Generating the Delaunay Mesh . . . . .	47
5.2.3 Creating the Prism layer . . . . .	47
5.3 ANSYS Turbo Pre: Preparation for Numerical Computation . . . . .	48
<b>6 Numerical Results</b>	<b>51</b>
<b>7 Conclusions</b>	<b>57</b>
7.1 Characteristics of the Indalma turbine . . . . .	57
7.2 Regions of losses . . . . .	58
<b>8 Recommendations</b>	<b>61</b>
<b>Bibliography</b>	<b>63</b>
<b>Appendices</b>	<b>69</b>
<b>A Compilation of accumulated data</b>	<b>71</b>
<b>B Used scripts and Arduino sketch</b>	<b>77</b>
B.1 lerArduino.sh . . . . .	77
B.2 tail.sh . . . . .	77
B.3 splitArduinoData.sh . . . . .	78
B.4 arduinoScript.ino . . . . .	78
<b>C ANSYS CFX Report</b>	<b>83</b>

# Introduction

“ You do it today  
because today is yesterday's tomorrow.

— **SpongeBob**  
(SpongeBob SquarePants)

## 1.1 Introduction

Turbines manufactured by Indalma Industries Inc. (3I) are developed for decentralized unattended power generation for isolated/remote communities (in the Brazilian Amazon hinterland), suitably adapted to the local context. Since 2000 over 44 pico-, 12 micro- and 6 mini hydropower plants have been installed with 3I turbines in various communities in the central Amazon hinterland, summing a total installed capacity of 1.5 MWe, providing electrical power to more than 2,200 families (Els et al., 2010).

In Suriname, contrary to the abovementioned Brazilian situation, the deployment (rate) of small-scale hydropower (i.e., less than 1 MWe) is significantly lower as is evident from the fact that: (1) the Poeketi micro hydropower plant, which was built in the early 1980's, is no longer functioning, and (2) the only other mini hydropower plant, namely the one at Gran Olo Sula, is currently in the commissioning process and it has an installed capacity of 150 kW. Given the fact that 15% of the population, mainly situated in the Surinamese hinterland, does not have adequate access to reliable electrical power, as well as the rising price of oil, Suriname's small-scale economy coupled to a weak world economy, climate-change challenges (Verlaan et al., 2008), and the green image that the country wishes to promote internationally, it is paramount to, among other things, conduct research on (pico) hydropower for reliably and sustainably meeting local demand and accounting for the local context.

This report presents the results of an experimental assessment and numerical analyses of a pico hydro turbine manufactured by 3I. The study is part of an informal broader joint research program between the Anton de Kom University of Suriname (AdeKUS) and the University of Brasilia (UnB) on sustainable development; within this program the project specifically focuses on pico hydropower. Within said project, part of the experimental work was conducted in the thermofluids laboratory at UnB. Use was made of previous experiments and experience gained in 2012 from measurements done at AdeKUS on a somewhat larger pico hydro turbine from the same make. The numerical analyses were performed at AdeKUS with the aid of the commercially available program ANSYS CFX.

The turbine under scrutiny is a unit fabricated by the Brazilian 3I, and, based on its geometry, it can be classified as a Francis hydro turbine. Yet, it is distinct from a classical Francis turbine in the sense that it has neither inlet guide vanes (IGV's) nor a water distributor. In a hydropower plant which employs a typical Francis turbine, the rotational speed of the shaft is governed by

either a mechanical or an electronic control system, which either varies the area of the turbine inlet, thereby effectively varying the flow through the turbine, or regulates the load on the turbine shaft. In hydropower plants developed by 3I, no mechanical or electrical control system is used („Auto-regulating behavior of an Indalma hydraulic turbine in microhydropower plant (To be published)“).

## 1.2 Problem definition & Objective

To understand the performance of the turbine under different conditions its characteristics need to be determined. These characteristics, typically graphically depicting the functional relationship between, on the one hand the rotational speed of the shaft, and on the other hand either the power, flow or efficiency, are usually supplied by the manufacturer and they are based on actual tests. For the specific turbine under scrutiny however, these curves are unknown. Nonetheless, in the past, the unavailability of such curves has not hampered the deployment of such systems, see Subsection 1.1.

Additionally, knowledge of the so-called specific speed of the turbine facilitates an a priori selection of a suitable turbine given the site conditions (especially the available head and flow). To exemplify this, consider that a Pelton turbine is better suited for power conversion in relatively high-head-low-flow site conditions, as opposed to, say, a Kaplan turbine (Husain et al., 2008). As stated in Subsection 1.1, the specific speed of the turbine is unknown. Having defined the problems, the objectives of this work are twofold, viz.

- To design, build and commission a test facility which allows for measuring power output, rotational speed, flow rate and indirectly the efficiency, and specific speed in order to classify the 3I turbine,
- To assess the turbines self regulating capacity, given the absence of a governor,

Anticipating the outcome of the experimental phase yielding unexpectedly low efficiencies, numerical analyses of the flow field through the turbine were done,

- With as a goal to compute and subsequently visualize the flow field in order to identify regions of losses. Knowledge of the flow field is relevant if the turbine is to be modified for improved efficiencies.

## 1.3 Structure

This work is divided in two parts. Part I describes the experimental part of the project and Part II discusses the numerical analyses using the experimental results as a point of departure. In Part I, starting from a review of relevant theory, see Section 2, subsequent sections treat respectively the experimental facility and the design of experiments. Similarly, Part II starts by describing the applied numerical methodology, followed by the procedure to setup the simulations and concludes with post-processed results. Hereafter, the results are discussed in Sections 4 and 6, and final conclusions are drawn and recommendations for future work are made in Section 7.

# Part I

---

## Experimental Section



# Brief Overview

“ It takes two to lie—  
one to lie and one to listen.

— Homer J. Simpson  
(The Simpsons)

## 2.1 Hydro turbine classification

Hydro turbines, alike all rotating fluid machinery, can be classified in different ways, namely on the basis of (1) energy transfer, (2) the geometry of the flow path, and (3) the specific speed. These are collaborated as follows (Husain et al., 2008):

### 1. Classification based on energy transfer:

[a] Action/Impulse turbines: in impulse turbines, if friction and effects due to gravity are neglected, the fluid pressure and the relative velocity do not change as the fluid passes over the blades. Impulse turbines do not run full of fluid and do not need a draft tube, i.e., the outlet tube, which is submerged in water. Furthermore, colloquially, impulse turbines are high head low flow turbines.

[b] Reaction turbines: in reaction turbines both the pressure and the relative velocity change over the rotor. Reaction turbines run fully filled with the working fluid and therefore need a draft tube which is fully submerged in water (such turbines should always be filled with water) (Harvey et al., 2013). Furthermore, colloquially, reaction turbines are low head high flowrate machines.

### 2. Classification based on geometry of the flow path

[a] Radial flow turbines: hereby the fluid flows in a plane that is partially or fully perpendicular to the axis of rotation.

[b] Axial flow turbines: hereby the fluid flows partially or fully parallel to the axis of rotation.

[c] Mixed flow turbines: in these turbines the fluid flows in a radial and axial direction. These turbines encompass a variety of designs between the extremes of fully radial and fully axial flow machines.

- Classification based on specific speed: the specific speed is usually supplied by the turbine manufacturer, but if unknown, one could acquire the specific speed experimentally. In this regard one determines whether the turbine is in the Pelton-, Francis- or the Kaplan range. The specific speed will be discussed in the next paragraph.

The specific speed ( $\Omega_s$ ) is an expression which relates the inlet head ( $H$ ), the volumetric flow rate ( $\dot{Q}$ ), and the rotational speed ( $\Omega$ ) as written in Equation 2.1 (Dixon and Hall, 2010), and it can be applied in two ways. Equation 2.1 is primarily used to select the most suitable rotating flow machine for a given set of conditions. Substitution subsequently yields the most suitable turbine type at its best operation condition or best efficiency point (BEP) (Harvey et al., 2013):

$$\Omega_s = \frac{\Omega \dot{Q}^{\frac{1}{2}}}{(gH)^{\frac{3}{4}}} \quad \left[ \frac{\text{rad}}{\text{s}} \right] \left[ \frac{\text{m}^3}{\text{s}} \right] \quad (2.1)$$

$$= \frac{\Omega \dot{Q}^{\frac{1}{2}}}{\left[ \frac{\text{m}}{\text{s}^2} \right] [\text{m}]} \quad \left[ \frac{\text{m}^3}{\text{s}} \right]$$

Conversely, by inserting the values at BEP into Equation 2.1 a turbine can be classified by using a graph which corresponds to the used equation. Care must be taken to establish which units must be used, because in various literature specific speeds with different units are often encountered. The units used for the specific speed in this report are as shown in Equation 2.1 and the used graph is Figure 2.1

Hydropower plants can be categorized in different classes based on the power output range, see Table 2.1<sup>1</sup>. The range is not unequivocally defined; worded differently the latter implies that different sources give somewhat different ranges.

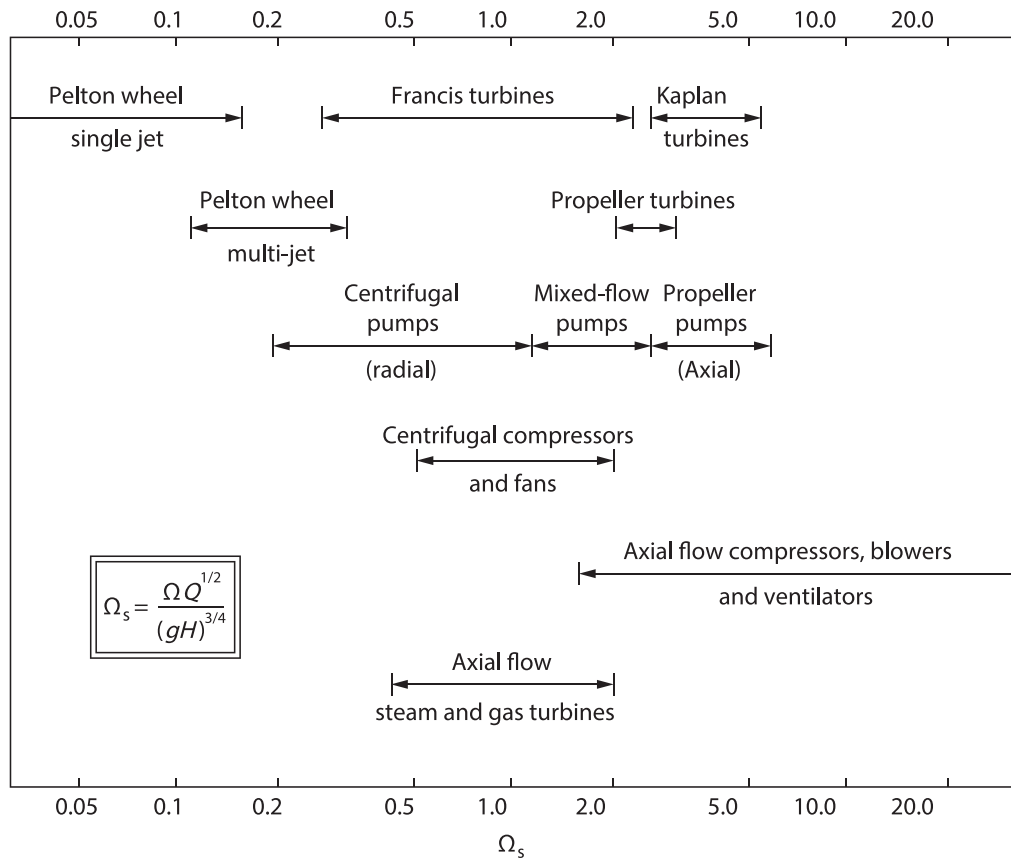
Hydro classification	Power range (kW)		Number of homes powered		
Pico	0	–	5	0	–
Micro	5	–	100	5	–
Mini	100	–	1,000	100	–
Small	1,000	–	10,000	1,000	–
Medium	10,000	–	100,000	10,000	–
Large	100,000+		100,000+		

Table 2.1.: Hydropower plant categories <sup>1</sup>.

## 2.2 Characteristics of hydro turbines

In hydro turbines momentum is transferred from continuously flowing water by a dynamic action with moving blade rows. Such a machine basically consists of a rotating part known as the rotor or runner, that delivers positive work by using the energy of the moving water (Raabe, 1985). Note that one of the objectives of this work is to determine the characteristics of the investigated turbine. To facilitate the discussion in this regard, knowledge of the theoretical performance

<sup>1</sup>Renewables First.



**Figure 2.1.:** Range of Specific Speeds for Various Types of Turbomachinery (Dixon and Hall, 2010).

characteristics of hydro turbines in general is needed. The theoretical curves can then be used as a benchmark for the experimental results.

Hydro turbine characteristics, typically graphically depicting the functional relationship between, on the one hand the rotational speed of the shaft, and on the other hand either the power, flow or efficiency, are usually supplied by the manufacturer and they are based on actual tests. For the specific turbine under scrutiny however, the curves are unknown. Nonetheless, in the past, the unavailability of such curves has not hampered the deployment of such systems, see Subsection 1.1.

### 2.2.1 Pelton Wheel

The Pelton Wheel is an impulse turbine which has one or more nozzles discharging jets of water which strike a series of buckets mounted on the periphery of a circular disc, see Figure 2.2.

In large hydropower installations, Pelton wheels are normally only considered for heads above 150 m. For small-scale pico- and micro-hydropower applications however, the Pelton wheels are used at much lower heads. For example, a small diameter Pelton wheel can produce up to a kW on a head of 20 m (Harvey et al., 2013). Pelton wheels do not need submerged draft tubes and

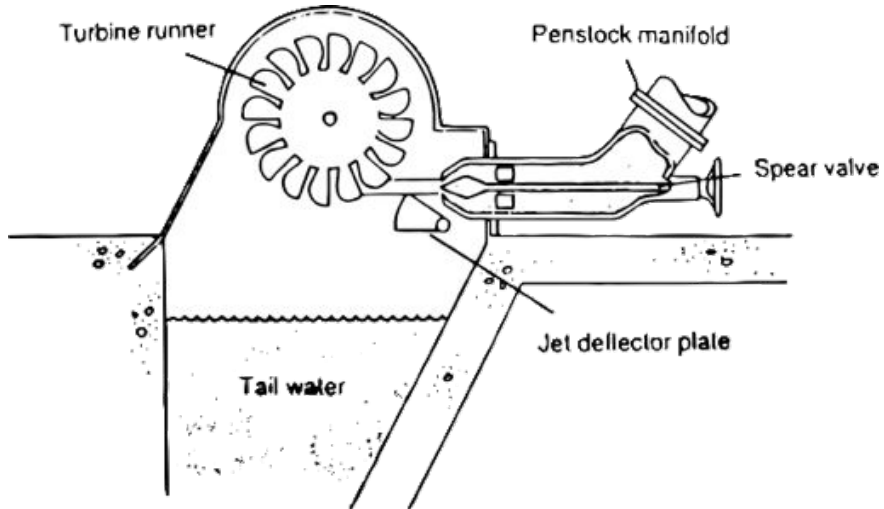


**Figure 2.2.:** Pelton wheel.  
Single-jet horizontal axis Pelton turbine.

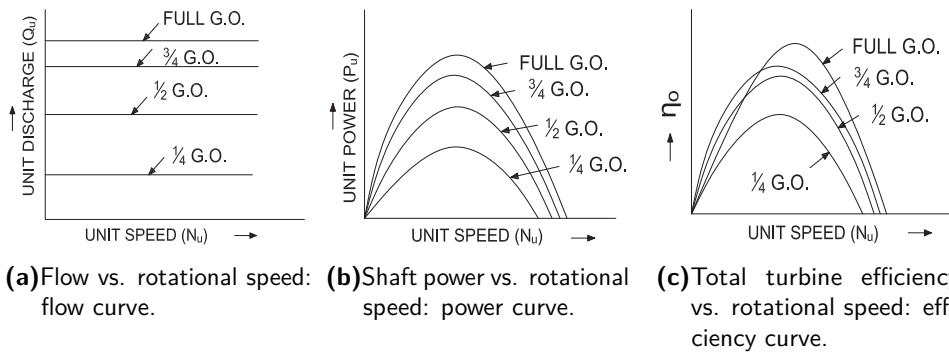


**Figure 2.3.:** Constant head characteristics of a Pelton turbine (Bansal, 2007).

are radial flow turbines which, compared to the other turbine types, have the lowest specific speeds. The constant head characteristics of a Pelton wheel are shown in Figure 2.3.

## 2.2.2 Kaplan Turbine

In small-scale hydropower, reaction turbines are more sophisticated to fabricate (Harvey et al., 2013). An example of a reaction turbine type is the Propeller turbine, see Figure 2.4. It has a rotor which acts like a ship's propeller, but in reverse. Kaplan turbines are propeller turbines which have swiveling blades. This improves the efficiency, but increases the manufacturing cost of the turbine (Dixon and Hall, 2010).

A characteristic of Kaplan turbines is that they are equipped with so-called guide vanes or wicket gates, which create a swirl in the axial flow, adapted to the runner to reduce flow losses. The Propeller or Kaplan turbines generally rotate at higher speeds, thus also have higher specific speeds compared to other turbine types and are more suitable for low heads. The higher speeds can sometimes eliminate the need for a transmission ratio, this implies lower overall costs. All

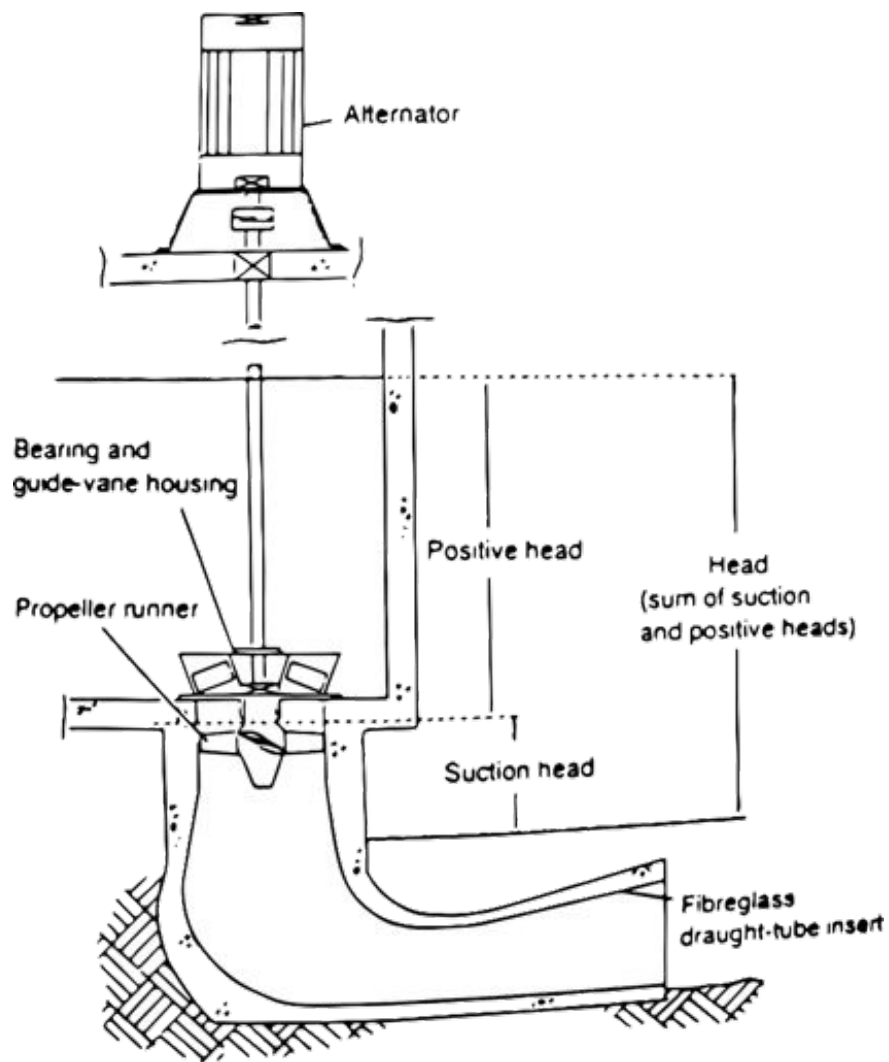


**Figure 2.4.: Kaplan turbine.**  
Micro hydro vertical shaft Kaplan turbine.

reaction turbines can be subjected to cavitation and need a draft tube which is fully submerged at all times, so that the turbine is always fully filled with water. This reduces the risk of cavitation, and increases the efficiency (Harvey et al., 2013).

The flow curve and the power curve of the Kaplan turbine at constant head are shown in Figure 2.5 with different inlet gate openings.

### 2.2.3 Francis Turbine

Francis turbines are reaction turbines that have a relatively complex runner blade profile and have a scrolled casing. This distributes water around the entire perimeter of the runner. Francis turbines are always fitted with guide vanes (shown in Figure 2.6). These regulate the mixed flow as it enters the runner, and are usually linked to a governor system that matches the water flow to the turbine loading (Harvey et al., 2013).

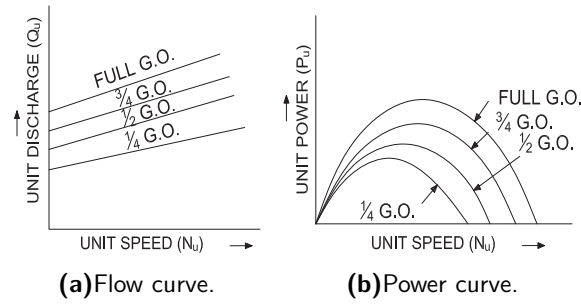


**Figure 2.5.:** Constant head characteristics of a Kaplan turbine (Bansal, 2007).

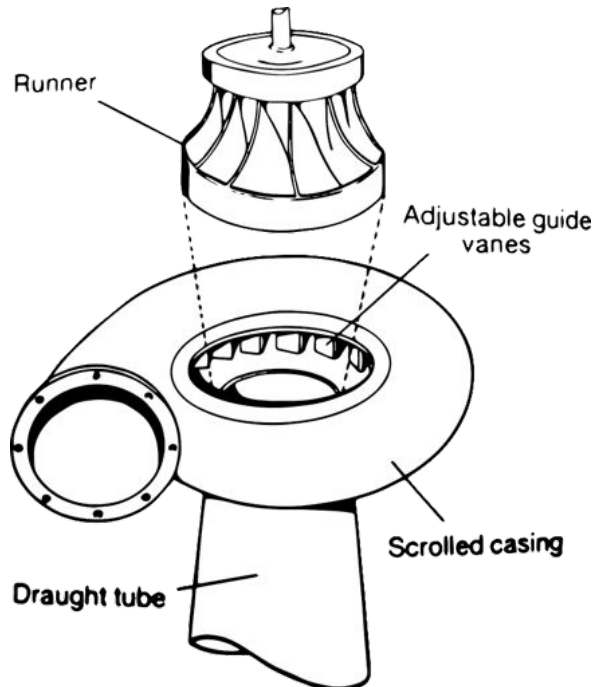


**Figure 2.6.:** Francis turbine  
Micro hydro vertical shaft Francis turbine.

The majority of Francis turbines are suitable for medium heads and are also subject to the danger of cavitation. A fully submerged draft tube also increases the efficiency and decreases the risk of cavitation for this turbine. Francis turbines cover a wide range in the spectrum of specific speeds between respectively the outer and inner range of the Pelton- and Kaplan turbines, see Figure 2.1. The constant head characteristics of the Francis turbine at different gate openings are shown in Figure 2.7.

## 2.3 Turbine control

Small-scale turbines, particularly those with a power output of the order of a hundred kW or less, often do not have a control system to maintain a relatively constant rotational speed (Harvey

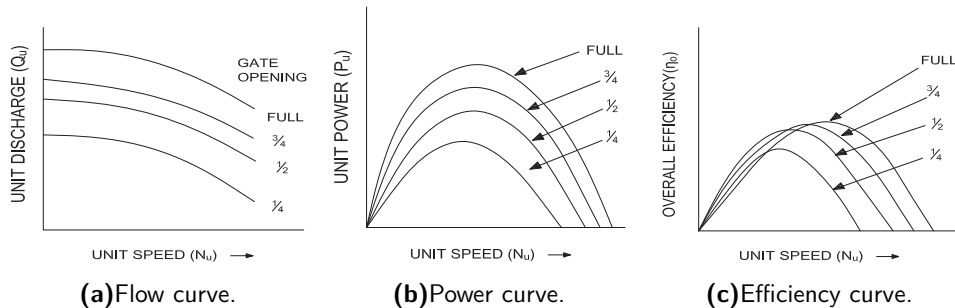


**Figure 2.7.:** Constant head characteristics of a Francis turbine (Raikar, 2012).

et al., 2013). Nevertheless, turbines require some form of control (be it electronic or mechanical) for the following reasons:

- Maintaining the frequency and voltage within acceptable limits, both of which are dependent upon the rotational speed of the turbine shaft, and
- Avoiding damage due to overspeed: runaway or runoff speed is a critical point at which the maximum speed of the turbine is reached. If a generator coupled to the turbine is not protected against runaway, it might be severely damaged along with other parts of the hydropower plant.

Having said that, in the field however, manual control is applied using one of the two methods described hereinafter (both procedures unavoidably influence the power output):

- Flow modification: here, by monitoring the voltage and frequency with respect to a set point range, an operator modifies the flow through the turbine via a hand-operated regulating valve.
- Load modification: here, energy is dissipated through a ballast load, e.g., a series of light bulbs or a heat element in air or water, which is connected to the generator to maintain a constant electrical load. The ballast load is manually adjusted by an operator on the basis of a voltage and frequency monitor.

Remark that turbines are very responsive machines, often capable of going from an underspeed condition to full overspeed (such a case can occur if for example the grid fails) in around a second, and they can thus easily get damaged if manual control is inappropriately applied. The risks of runaway can be minimized in various ways. One method is based on modifying the flow through the turbine. This is a form of overspeed braking which is incorporated into the turbine. For example, shrouds are sometimes fitted to Pelton wheels, which spoil the performance at overspeed, thereby reducing the runaway speed to around 130% of the nominal speed. However, there are performance and cost penalties (Harvey et al., 2013). Another method is based upon the operation on the back side of the power curve and it is referred to as such. The principle behind this control method is based on a negative feedback loop between the turbine power curve and the system (e.g., piping) characteristics. With this control method the conventional way of selecting the operating point at maximum power of the parabolic power curve is avoided,

namely by shifting the operation point to 75% of the runaway speed (Harvey et al., 2013), and thereby facilitating the possibility of the naturally occurring negative feedback (worded differently this implies operating on the right-hand side of the parabolic power curve, thereby setting the operating point on the downwards sloping part of the power curve). By doing so, the manual adjustment of the turbine is less frequent and the maximum frequency variation due to overspeed is reduced to about  $\pm 33\%$  of the nominal speed. This variation of frequency might still be large, but it permits full use of the plant capacity without manual control and without risk of damage. An automatic voltage regulator (AVR) is required to avoid excessive voltage variation and this method is only suitable for impulse machines. Reaction machines however, when controlled using the operation-on-the-backside-of-the-curve method, may suffer from cavitation because the turbine must be capable of operating continuously near its runaway speed (Harvey et al., 2013). Figure 2.8 illustrates the latter mentioned overspeed protection method.

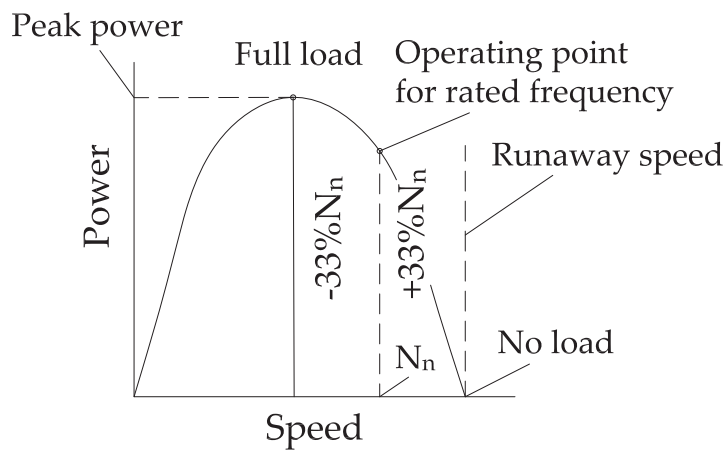


**Figure 2.8.: A method for reducing overspeed risks.**  
Operation on the back side of the power curve method.

The turbine used in this study is in the pico range, since its rated output power is less than 5 kW. Moreover, in the field, the operation-on-the-back-side-of-the-power-curve method is used in hydropower plants with this turbine.

# Experimental Setup

**“** Just when I thought you couldn't possibly be any dumber,  
you go and do something like this... and totally redeem  
yourself!

— Harry Dunne  
(Dumb & Dumber)

## 3.1 Commissioning of the test facility and design of experiment

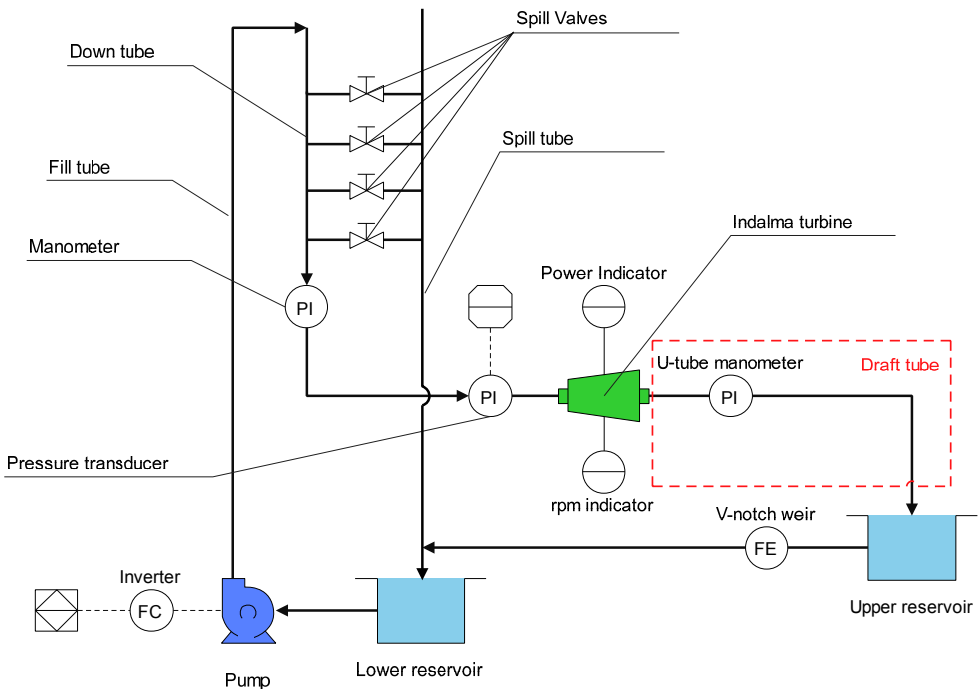


**Figure 3.1.:** Schematic overview of the experimental test setup.

Figure 3.1 shows a schematic overview of the experimental test setup. The facility was designed and built from the ground up, at FGA, by a team of workers and students, including the authors. Its intended use is to test various pico- and micro turbine designs over a wide range of parameters encountered in the field, like the head at the inlet, the rotational speed of the shaft, the fluid flow rate, and the pressure at the exit of the turbine, specifically if the turbine is equipped with

a draft tube.

With reference to Figure 3.1 the sequence of processes is as follows: (1) water is pumped from the *lower reservoir* to the *fill tube* and into the *down tube*. (2) If required, part of the water can be spilled through one of the *spill valves* into the *spill tube* and from there, back into the *lower reservoir*. (3) The remaining water in the *down tube* follows a path which leads to the turbine. (4) Depending on whether the *draft tube* (located in the red rectangle) is submerged in water or not, the water exiting the turbine is respectively guided directly into the water in the *upper reservoir* or it is spilled onto the water surface contained in the *upper reservoir*. (5) Due to gravity, water flows from the upper reservoir to the *lower reservoir* thereby completing the cycle. Note that the spilling was required to measure the flow rate using a *V-notch weir*.

Furthermore, the test facility is equipped with instruments listed hereunder to either simulate and manipulate or measure respectively said field parameters or performance output variables:

- An inverter-controlled pump: the pump creates the necessary flow and head through the turbine and with the aid of the inverter these parameters can be varied nearly smoothly,
- Spill valves: these are parts of the piping arrangement that, in combination with the inverter, allow for varying the head at the turbine inlet,
- A de Prony brake: an instrument used for measuring the power output at the shaft; this instrument is discussed in due course,

A rotational speed sensor,

Strain gauges: these are used to measure forces produced by the turbine from which the torque can be deduced,

- A V-notch weir: an instrument used for water flow measurements; this instrument is discussed in due course,
- Pressure gauges (both analog and digital instruments were used): these measure the pressure at various parts of the facility to acquire therefrom the head and efficiency of the turbine.

Due to the archival value of this work, an exhaustive description of the instrumentation and the data acquisition (DAQ) system is given in the sections hereinafter, and the used programs are presented in Appendix B.

## 3.2 Instrumentation

### 3.2.1 Flow- and Head-control

The flow and the head at the inlet of the turbine are controlled with an inverter and the spill valves. The inverter is a WEG CFW09, and it is computer controlled using the "superdrive" software. The inverter can vary the rotational speed of the pump, which is responsible for the

flow through the system i.e., piping plus valves plus turbine, to at least 1 rpm. The inverter is shown in Fig. 3.2.



**Figure 3.2.:** The WEG CFW09 inverter.

### 3.2.2 De Prony brake

A de Prony brake is a dynamometer which uses friction to measure the amount of torque produced by the turbine at the shaft. It consists of 2 spring balances, a friction belt and a water-cooled drum mounted on the turbine shaft (see Figure 3.3). For a more accurate measurement, two (2) strain gauges were added and the force values were taken from these instruments. To calculate the power output of the turbine, the rotational speed was determined using a proximity sensor. The properties of the strain gauges and the proximity sensor are discussed next.

#### De Prony brake sensors

A strain gauge uses a piezoelectric electric sensing element to measure the deflection of a material. The measured deflection can then be correlated with the force needed to deflect the material. The used model of the strain gauges is manufactured by MK Controle and has the model number CSAZL-20. This model can measure up to a weight of 200 N. The input voltage can vary anywhere between 9 V and 12 V with an uncertainty of 0.07%. The uncertainty in the measurement of forces with the selected strain gauges, including the DAQ system, is 0.2 N. The proximity sensor is a JNG LM8-3002NA. The frequency range of this model is 25–500 Hz, the input voltage can vary anywhere between 6 V to 36 V and the voltage drop in the sensor is less than 3 V. The detection distance was from 0–2 mm.

Proximity sensors can detect the presence of metal without any physical contact within the detection distance. A metal piece or pickup (in this case a bolt which secured the shaft collar) was the only point on the turbine shaft where the gap was smaller than 2 mm. This meant that

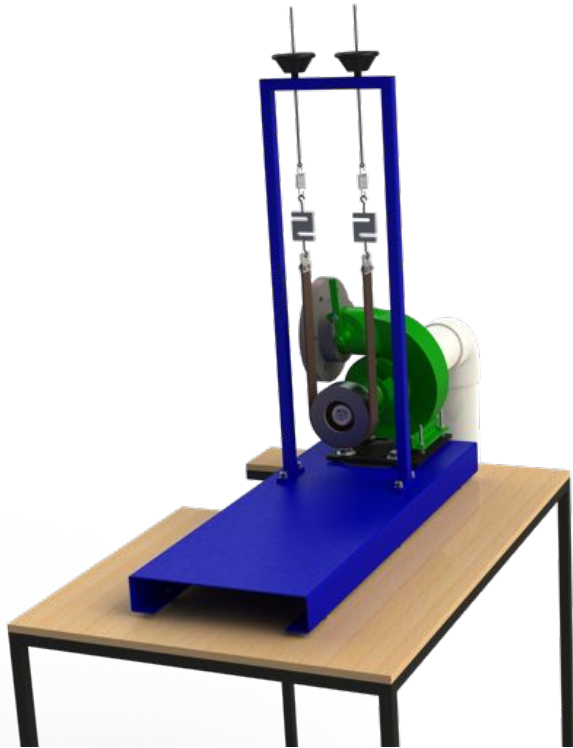


**Figure 3.3.: De Prony Brake.**

the proximity sensor would switch to the "on position" every time the bolt reached the proximity sensor and off again once it passed the sensor. By clocking the time between "on positions" the rotational speed can be obtained. This method of measuring the rotational speed is very accurate, but due to limitations with the DAQ system the uncertainty in the rotational speed of the turbine is 5 rpm.

In Fig. 3.4 the proximity sensor and the bolt (used as pickup) are shown in an off position.

### 3.2.3 Flow rate measuring instrument

The flow rate was measured with a V-notch weir (refer to Fig. 3.5). This instrument had the disadvantage that the measurement of the flow could not be instantaneous. To have reliable data, measurements were taken at a time interval of 60 seconds (see Subsection 3.3.4). The uncertainty of this instrument was 0.2 l/s.

### 3.2.4 Pressure measuring instruments

The test setup consisted of one pressure transducer and two manometers. The pressure gauge was located at the inlet of the hydro turbine. The gauge is of the WIKA instruments brand and has a range of up to 2.5 bars with an uncertainty of 5 mbar including the error of the DAQ system. The sensor has an input voltage that can vary anywhere between 8 V and 30 V and an output current between 4 mA and 20 mA. The pressure transducer was attached to the test setup with multiple holes over a cross-section in order to obtain a stable static pressure



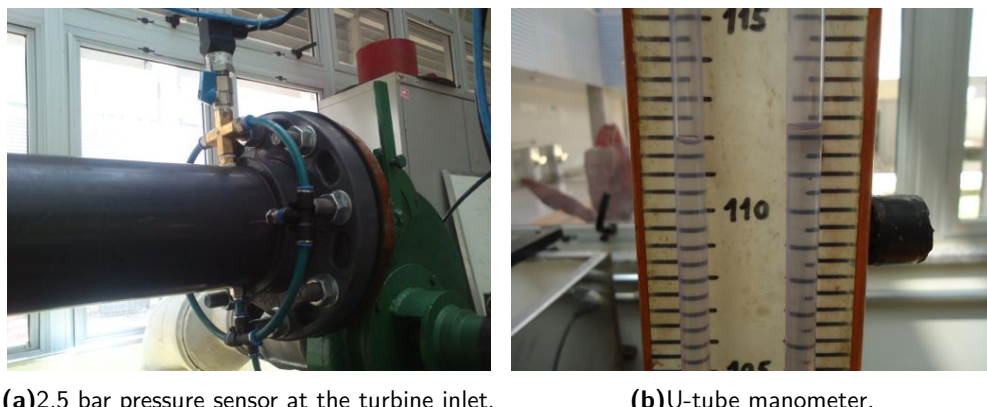
**Figure 3.4.:** Rotational speed sensor.



**Figure 3.5.:** The V-notch flow measurement instrument.

measurement. Figure 3.6a displays the pressure sensor mounted at the turbine inlet. During earlier tests, a negative pressure was noticed in the turbine outlet. The digital instruments available at the laboratory, at that time, did not support negative pressure measurements. Hence, an open U-tube manometer was mounted at the turbine outlet. Figure 3.6b is a picture of the U-tube manometer which measured the pressure at the turbine outlet. To measure the head on the turbine inlet, a manometer was mounted with a tee on the downtube (see Figure 3.1) and indicated the water level in this tube. The maximum head that could be measured with the manometer was 7 m. And the tee made it possible to add a pressure

transducer as an alternative to measure heads exceeding 7 m. During the tests however, the pressure transducer was broken and therefore heads exceeding 7 m were not applied.



(a) 2.5 bar pressure sensor at the turbine inlet. (b) U-tube manometer.

**Figure 3.6.:** Pressure measuring instruments.

### 3.3 Data acquisition systems

To acquire the data measured by the sensors two DAQ systems were used, viz.: (1) CW552 kit DAQ and (2) the Arduino based DAQ. Refer to Figure 3.7 for a schematic view of both systems. The abovementioned DAQ systems are discussed in more detail in respectively Subsections 3.3.1 and 3.3.2. The reason for choosing two separate systems was simply because of the fact that the CW552 kit was already present/built at the time of the start of this project.

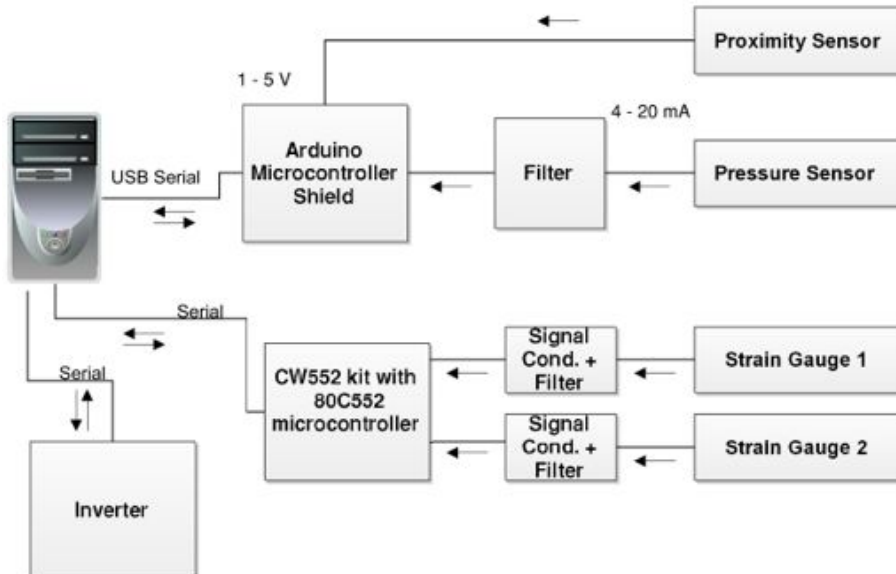


**Figure 3.7.:** Data Acquisition system diagram.

### 3.3.1 CW552 kit DAQ

In order to receive and convert the data from the strain gauges, a CW552 kit was used. The microcontroller's software and hardware characteristics allow for usage with 64 kb of data memory and it has an 8-bit resolution.

The microcontroller is equipped with both analog and digital I/O ports, a power supply and a liquid crystal display (LCD). The kit also has an RS232 serial interface for communication, which is used to send configurations to the microcontroller and to receive data from it. The kit was originally made to measure the rotational speed and strain gauge data, but the rotational speed data was migrated to the Arduino board for more accurate and more frequent measurements.

In Figure 3.8 a picture of the CW552 kit is shown.

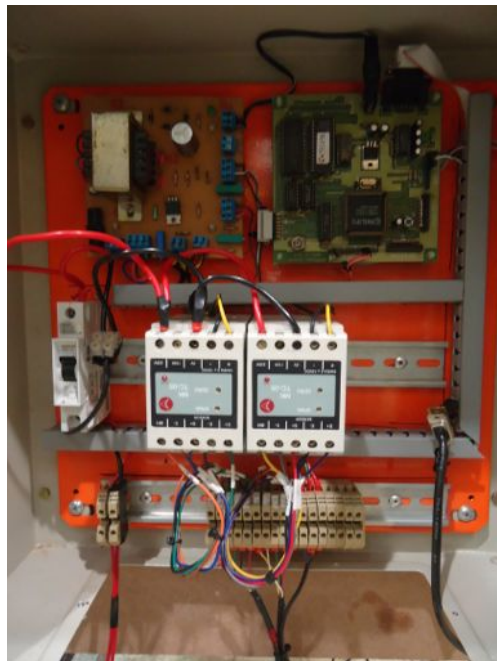


Figure 3.8.: CW552 kit DAQ system.

### 3.3.2 Arduino based DAQ

Arduino is an open-source electronics prototyping platform based on flexible, easy to use hardware and software. The Arduino hardware has a microcontroller which is relatively easy to program with a simple file called a sketch, generated by the Arduino software with a language similar to the C programming language.

There are many different Arduino models available. The Arduino Uno R3 model was chosen purely because of its availability. The Uno (refer to Figure 3.9) has an ATmega32u4 microcontroller with a 10-bit resolution. The specifications of the Arduino Uno were more than sufficient for the testing purposes (the Arduino Uno could arguably replace the CW552 kit mentioned above). Data was sent to and received from the Uno using its USB connection, which emulates a serial port.



Figure 3.9.: Front view of the Arduino Uno.

A circuit board on which the Arduino Uno could be integrated (also known as a shield) was made. This shield contains four input ports, on which, in the future, multiple pressure sensors can be connected. It also contains four current-to-voltage converters to condition the pressure sensor's output for the Arduino Uno input. There were also two input ports, on which interruption based sensors can be connected (such as the proximity sensor and various water flow sensors). Lastly, an LCD screen is accommodated and all of the mentioned components are powered by this board. See Figure 3.10 for a picture of the shield made for the Arduino Uno.

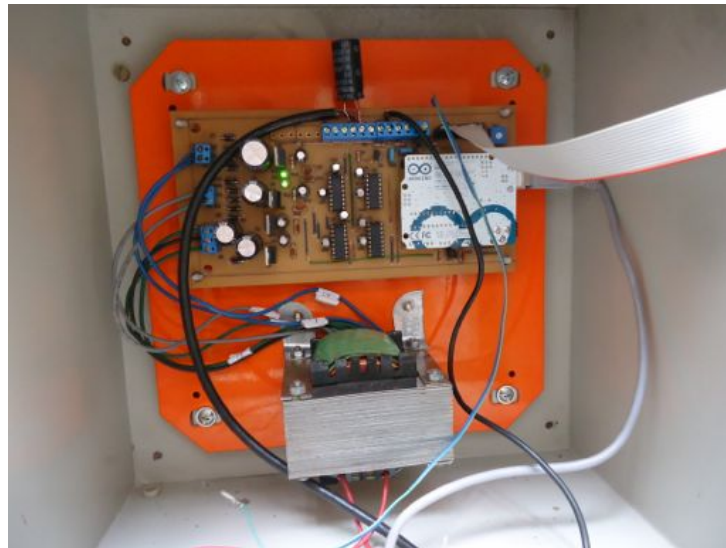


Figure 3.10.: Arduino shield for DAQ.

### 3.3.3 Filtering the output data

The output voltage of the pressure sensors showed interference. This was detected with an oscilloscope and was identified to be due to an electric field emitted by the inverter. The interference was resolved with a  $2000 \mu\text{F}$  capacitor connected in parallel with the pressure sensor.

### 3.3.4 Response of the test facility

In order to accurately collect experimental data from the hydro turbine the total response of the system had to be determined. This means that it is needed to determine the maximum time which is required for each parameter to reach a steady state value within a variation of at most 2%, after a disturbance of at most 20% is applied.

The percentages used above have been determined experimentally. The procedure to determine the response was done in the following way:

1. At first, the input parameters were identified. These are all the parameters, which, if modified, cause other variables to change, e.g., if the belt tension  $F_s$  of the de Prony brake is changed, the shaft speed of the turbine ( $n$ ) consequently varies.
2. A series of measurements were done, whereby each parameter is independently varied one at a time, according to the aforementioned 20% criterion. The required time for the variables to reach a steady state of within 2% variation then constitutes the response time of the corresponding variable.
3. The maximal value in the array of response times gathered in the previous step, is then presumed to be the slowest response time of the system.

From experiments it was found that the slowest response time emerged from the V-notch, and was around 40 seconds. To ensure reliable data a waiting period of circa a minute was used between measurements.

## 3.4 Measurement procedure

The measurement procedure focused on acquiring data to calculate the differential energy potential across the turbine. The equation used for the calculations was derived from the general steady-flow energy Equation 4.1. Furthermore, the water head at the inlet of the turbine was kept constant. This was to approximate the conditions in which such a turbine should operate once installed in the field. The procedure consisted of the following steps starting from the no-load state:

- The U-tube manometer was set to zero if needed and the head manometer's valve was closed,
- Only thereafter the pump could be started using the inverter's "superdrive" software once the turbine was at a no-load state,
- The data acquisition system was initiated/started,
- After visual inspection and confirmation that there were no air bubbles in the inlet of the turbine (worded differently this is to say that there was a full flow through the turbine) the head manometer's valve was opened and its value was adjusted to the desired head using

the inverter. Note that initially the inverter was intended for flow control and that the spill valves would be used for head control. However, due to complications with unintentional air entrainment in the system, in the end, the position of the opening of the spill valves remained unaltered and head control was done using the inverter.

- Once the desired head was reached and appeared stable, a waiting period of one minute was used,
- Thereafter, the first measurements, which were at a no-load condition, i.e., the belt of the de Prony brake was loose, were taken.
- The measurement procedure was as follows:
  1. Variables were logged manually namely: (1) the head, (2) the outlet pressure and (3) the water level in the upper reservoir.
  2. The rotational speed, inlet pressure and strain gauge data were logged automatically,
  3. After all the data were recorded, a new measurement point was set by adjusting the tension of the de Prony brake friction belt,
  4. The belt tension changed the load on the turbine, which changed the head across the turbine. This was readjusted to the desired height, again, using the inverter,
  5. After one minute, this procedure was repeated.
- The measurement procedure according to the enumerated items hereabove was repeated until the turbine stopped rotating, i.e., at maximum load of the turbine.

These measurements were done twice, with and without fully submerged draft tube, at 7 m, 5.5 m and 4 m. In the next section, the experimentally acquired data will be shown.

# 4

## Experimental Results & Discussion

“ I'm not insane,  
my mother had me tested!

— Sheldon Cooper, B.S., M.S., M.A., Ph.D., Sc.D.  
(The Big Bang Theory)

### 4.1 Raw data

As mentioned in the previous subsection, measurements were taken in duplex at different water heads and different turbine outlet conditions. Only four tables with experimentally acquired data are presented in this section. The total of twelve data sets are presented in Appendix A. Labels clearly indicate which data are measured and which data are computed using the appropriate equations presented hereinafter.

The strain gauge data were calculated with Equation 4.1. This equation was derived from the calibration data.

$$S = ((S_{\text{raw}} - 0.186) + 0.018)g \quad (4.1)$$

The shaft power [W] was calculated utilizing Equation 4.1.

$$P = |S_1 - S_2| \times r_{\text{drum}} \times n \times \frac{2\pi}{60} \quad (4.2)$$

The inlet pressure data [cm H<sub>2</sub>O] were calculated using Equation 4.1. This equation was derived from the calibration data sets.

$$p_{\text{inlet}} = (p_{\text{raw}} \times 2.5472) - 1.7877 \quad (4.3)$$

The outlet pressure data [cm H<sub>2</sub>O] were determined by subtracting the water levels in the left side of the U-tube manometer with the levels in the right side, i.e.,  $p_{outlet} = manometer_{right} - manometer_{left}$ <sup>1</sup>.

$$\hat{h}_1 + \frac{1}{2}V_1^2 + gz_1 = (\hat{h}_2 + \frac{1}{2}V_2^2 + gz_2) - q + w_s + w_v \quad (4.4)$$

Lastly, the equations to determine the following efficiencies were derived from Equation 4.1 (White, 2011) and were subsequently simplified to Equations 4.1, 4.1 and 4.1 (Husain et al., 2008), respectively for the hydraulic, mechanical and total efficiency.

$$\eta_{hydr} = \frac{\text{power developed by runner}}{\text{hydraulic power}} = \frac{\gamma \dot{Q} E}{\gamma \dot{Q} H} \quad (4.5)$$

$$\eta_{mech} = \frac{\text{power developed at turbine shaft}}{\text{power developed by runner}} = \frac{P}{\gamma \dot{Q} E} \quad (4.6)$$

$$\eta_{tot} = \frac{\text{power developed at turbine shaft}}{\text{hydraulic power}} = \frac{P}{\gamma \dot{Q} H} \quad (4.7)$$

Table 4.1 is one of the two data sets at 7 m (inlet) head with a submerged draft tube, i.e., the turbine outlet is submerged in the water contained in the upper reservoir. The highest power output and greatest water flow rate were measured at this height and with this turbine outlet condition.

Table 4.2 shows a series of measurements done at 5.5 m (inlet) head again with the draft tube submerged in water. The highest total efficiency was measured at this height and with this turbine outlet condition.

Table 4.3 shows a measurement series performed at 4 m (inlet) head with a submerged draft tube. Notice that in all the measurements with a submerged draft tube, some data points have negative outlet gauge pressures (that is to say there exists an under-pressure). Remark that, int. al, the influence on the power output as a function of the depth of the discharge into the water and the geometry of the draft tube was not investigated.

Table 4.4 shows a measurement conducted at 4 m (inlet) head whereby the water exiting the turbine is discharged above the water surface. Measurements done without a submerged draft tube did not exhibit negative outlet gauge pressures. What is more, measurements without a submerged draft tube consistently exhibited lower power outputs and lower efficiencies.

---

<sup>1</sup>Simply stated, this implies the manometer is used correctly.

	Water Level (m)	Rotational Speed (rpm)	Strain Gauge 1 (Raw)	Strain Gauge 2 (Raw)	Pinlet (Raw)	Manometer Left (m)	Manometer Right (m)	Total Head (m)	Flow Rate (/s)	Strain Gauge 1 (N)	Strain Gauge 2 (N)	Shaft Torque (Nm)	Shaft Power (W)	$\gamma_{inlet}$ (cm H <sub>2</sub> O)	$\gamma_{outlet}$ (cm H <sub>2</sub> O)	$\eta_{hydr}$ (%)	$\eta_{mech}$ (%)	$\eta_{tot}$ (%)
	Measured Data								Calculated Data									
0.234	1760	0	0	223.5	0.880	1.365	7.00	11.4	0.0	0.0	0	567	48.50	76.0	0.0	0.0		
0.243	1600	0	10	207.8	0.985	1.285	7.01	13.2	0.2	18.4	1	217	528	30.00	72.9	32.8	23.0	
0.253	1300	1	25	178.9	1.115	1.192	7.00	15.5	2.0	45.8	3	423	454	7.70	65.6	60.8	39.9	
0.257	1150	5	36	166.4	1.210	1.130	7.02	16.4	9.3	65.9	4	484	422	-8.00	63.1	67.8	42.8	
0.261	1050	18	55	162.7	1.272	1.094	7.00	17.4	33.0	100.5	5	527	413	-17.80	63.4	69.6	44.1	
0.263	830	21	65	148.9	1.263	1.100	7.03	17.9	38.5	118.8	6	495	378	-16.30	57.9	69.3	40.1	
0.264	580	37	91	141.7	1.260	1.101	7.00	18.2	67.7	166.2	7	425	359	-15.90	55.5	61.4	34.1	
0.265	320	56	116	138.3	1.257	1.104	7.02	18.5	102.4	211.8	8	260	350	-15.30	54.0	38.1	20.5	
0.265	160	67	132	137.9	1.230	1.120	7.02	18.5	122.4	241.0	8	141	349	-11.00	53.2	20.9	11.1	

Table 4.1.: Measurements at 7 m head with submerged draft tube.

Water Level (m)	Rotational Speed (rpm)	Strain Gauge 1 (RAW)	Strain Gauge 2 (RAW)	Pieler (RAW)	Manometer Left (m)	Manometer Right (m)	Total Head (m)	Flow Rate (l/s)	Strain Gauge 1 (N)	Strain Gauge 2 (N)	Shaft Torque (Nm)	Shaft Power (W)	Pieler (cm H <sub>2</sub> O)	Portlet (cm H <sub>2</sub> O)	$\eta_{hydr}$ (%)	$\eta_{mech}$ (%)	$\eta_{tot}$ (%)
Measured Data								Calculated Data									
0.227	1580	0	0	174.9	0.955	1.290	5.50	10.1	0.0	0.0	0	444	33.5	77.0	0.0	0.0	
0.235	1460	7	14	164.3	1.015	1.245	5.50	11.6	12.9	25.7	1	139	417	23.0	74.0	30.0	22.2
0.243	1270	4	20	147.2	1.118	1.177	5.49	13.2	7.5	36.7	2	276	373	5.9	69.3	55.9	38.7
0.249	1070	8	31	133.6	1.206	1.125	5.50	14.6	14.8	56.7	3	334	338	-8.1	65.4	65.1	42.6
0.252	930	10	40	122.0	1.261	1.091	5.50	15.2	18.4	73.2	4	379	309	-17.0	61.7	74.8	46.1
0.255	830	13	46	116.4	1.270	1.077	5.50	16.0	23.9	84.1	4	372	299	-19.3	59.5	72.7	43.3
0.256	670	18	55	114.3	1.281	1.076	5.52	16.2	33.0	100.5	5	334	289	-20.5	58.5	65.7	38.4
0.257	500	25	67	108.0	1.272	1.085	5.50	16.4	45.8	122.4	5	285	273	-18.7	55.5	58.0	32.2
0.258	350	34	79	106.5	1.272	1.085	5.49	16.7	62.2	144.3	6	214	269	-18.7	54.9	43.4	23.8
0.258	170	47	94	106.9	1.256	1.094	5.49	16.7	85.9	171.7	6	108	271	-16.2	54.6	22.1	12.1

Table 4.2.: Measurements at 5.5 m head with submerged draft tube.

	Water Level (m)	Rotational Speed (rpm)	Strain Gauge 1 (RAW)	Strain Gauge 2 (RAW)	$\rho_{water}$ (RAW)	Manometer Left (m)	Manometer Right (m)	Total Head (m)	Flow Rate (l/s)	Strain Gauge 1 (N)	Strain Gauge 2 (N)	Shaft Torque (Nm)	Shaft Power (W)	$\rho_{water}$ (cm H <sub>2</sub> O)	Pointet (cm H <sub>2</sub> O)	$\eta_{hydr}$ (%)	$\eta_{mech}$ (%)	$\eta_{tot}$ (%)
	Measured Data									Calculated Data								
0.220	1360	0	0	127.1	1.035	1.235	4.00	8.9	0.0	0.0	0	322	20.0	78.8	0.0	0.0		
0.230	1160	4	12	110.8	1.125	1.175	4.02	10.6	7.5	22.1	1	126	280	5.0	71.8	41.9	30.1	
0.240	900	3	20	92.4	1.240	1.105	4.01	12.6	5.7	36.7	2	208	233	-13.5	64.9	64.6	41.9	
0.244	790	5	26	86.3	1.278	1.078	4.00	13.5	9.3	47.6	3	225	218	-20.0	62.8	68.0	42.7	
0.245	590	9	35	82.3	1.283	1.076	4.02	13.7	16.6	64.0	3	208	208	-20.7	60.1	64.3	38.7	
0.247	400	14	45	78.1	1.275	1.081	4.01	14.1	25.7	82.3	4	168	197	-19.4	57.3	53.0	30.4	
0.248	210	23	56	72.9	1.270	1.085	4.00	14.3	42.1	102.4	4	94	184	-18.5	53.9	31.1	16.7	
0.249	110	28	63	73.7	1.257	1.094	4.00	14.6	51.3	115.1	5	52	186	-16.3	53.9	17.0	9.2	

Table 4.3.: Measurements at 4 m head with submerged draft tube.

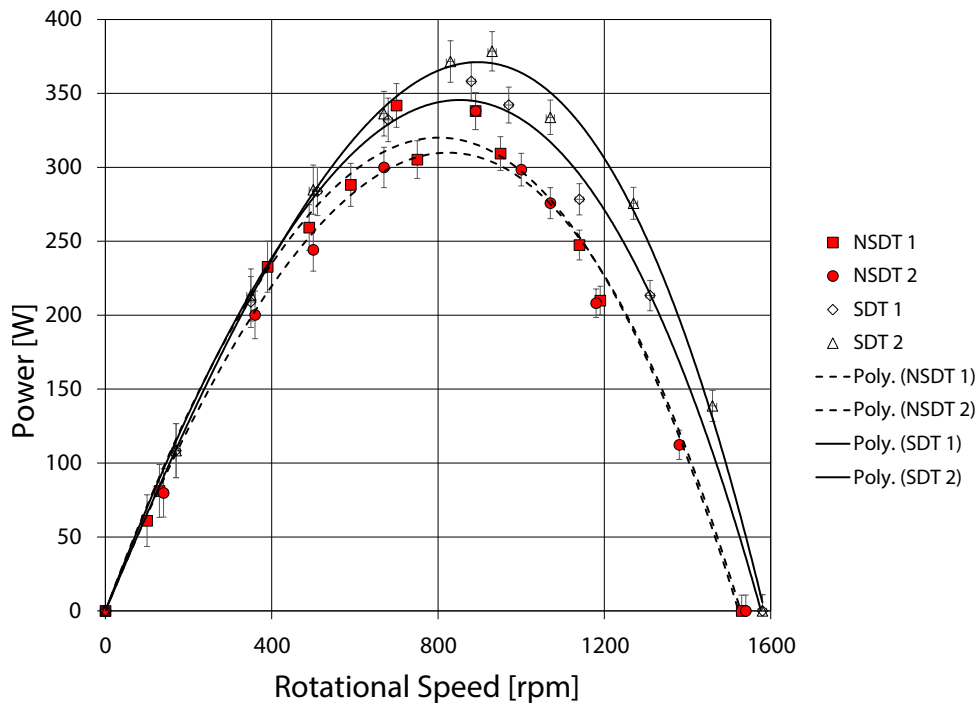
	Water Level (m)	Rotational Speed (rpm)	Strain Gauge 1 (RAW)	Strain Gauge 2 (RAW)	$\rho_{water}$ (RAW)	Manometer Left (m)	Manometer Right (m)	Total Head (m)	Flow Rate (l/s)	Strain Gauge 1 (N)	Strain Gauge 2 (N)	Shaft Torque (Nm)	Shaft Power (W)	$\rho_{water}$ (cm H <sub>2</sub> O)	Pointet (cm H <sub>2</sub> O)	$\eta_{hydr}$ (%)	$\eta_{mech}$ (%)	$\eta_{tot}$ (%)
	Measured Data									Calculated Data								
0.215	1300	0	0	130.0	0.970	1.270	4.00	8.0	0.0	0.0	0	329	30.0	78.1	0.0	0.0		
0.223	1120	3	8	118.8	0.987	1.256	3.97	9.4	5.7	14.8	1	76	301	26.9	72.3	28.8	20.9	
0.233	950	1	14	106.9	1.060	1.198	3.98	11.2	2.0	25.7	2	168	271	13.8	67.8	56.6	38.4	
0.238	760	3	21	93.0	1.129	1.164	4.00	12.2	5.7	38.5	2	186	235	3.5	61.2	63.5	38.8	
0.240	660	5	26	90.0	1.140	1.156	3.99	12.6	9.3	47.6	3	186	227	1.6	59.9	63.7	38.2	
0.242	480	9	36	86.8	1.105	1.180	4.00	13.0	16.6	65.9	3	176	219	7.5	56.1	61.2	34.4	
0.243	350	14	42	85.0	1.116	1.172	4.01	13.2	25.7	76.8	4	133	215	5.6	55.4	46.1	25.6	
0.243	130	24	54	83.0	1.095	1.184	4.00	13.2	44.0	98.7	4	53	210	8.9	53.5	19.1	10.2	

Table 4.4.: Measurements at 4 m head without submerged draft tube.

## 4.2 Processed data & Discussion

### 4.2.1 Submerged draft tube vs non-submerged draft tube

In Figure 4.1 the power curve of the turbine has been plotted at 5.5 m head and at two different turbine outlet conditions. A polynomial of the third order was used to fit these data points. A third-order polynomial was suitable because according to theory the power output is proportional to  $n^3$ . The dashed lines show results of a non-submerged-draft-tube condition and the continuous lines indicate the contrary. It follows from Figure 4.1 that the 3I turbine has a higher power output and consequently a higher total efficiency if the draft tube is fully submerged in water as opposed to a non-submerged case. Although only a single graph is shown, this is consistently observed with all of the investigated inlet heads.



**Figure 4.1.:** Comparison of power output between the submerged draft tube condition (SDT) and the non-submerged draft tube condition (NSDT).  
The data in the graph was acquired at a head of 5.5 m.

Figure 4.1 indicates that the 3I turbine is more likely to be a reaction turbine than an action turbine. Although the power and efficiency were considerably higher with a submerged draft tube, care should be taken when choosing a draft tube design, because according to (Harvey et al., 2013), the use of draft tubes for reaction turbines requires knowledge of its cavitation limits.

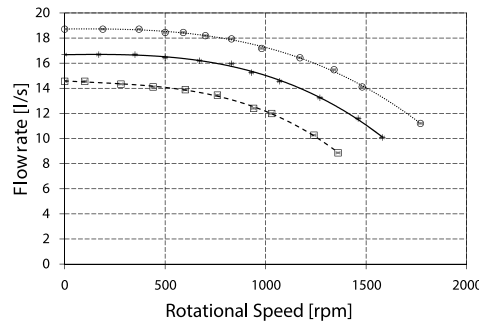


**Figure 4.2.:** Flow curve of the 3I turbine at different heads.

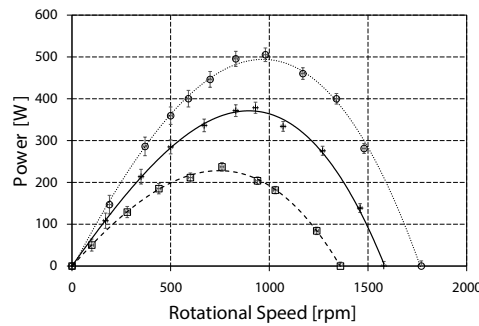


**Figure 4.3.:** Power curve of the 3I turbine at different heads.

## 4.2.2 Performance characteristics of the 3I turbine

### Best efficiency point

The total efficiency curves of the experimental setup with the 3I turbine have been plotted in efficiency hill curves shown in Figures 4.5 and 4.6. Figure 4.5 shows a fitted curve of the efficiency measured at three different heads, and Figure 4.6 shows a top view of the previously mentioned figure. This is also known as a contour plot, whereby points of the same color have the same efficiency (isoefficiency curves), with the highest efficiency or best efficiency point (BEP) being in the brightest purple area of the figure.

The BEP of the pico hydro 3I turbine (on the used experimental setup) was measured at a head of 5.5 m. The water flow rate and rotational speed at the BEP was used to calculate the specific speed of the turbine. This is discussed in the next section.

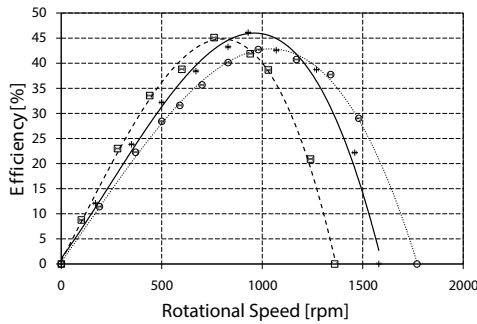


**Figure 4.4.:** Efficiency curve of the 3I turbine at different heads.

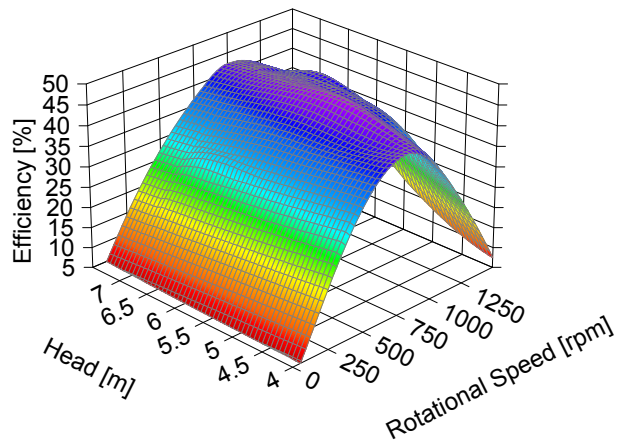


**Figure 4.5.:** Efficiency hill curve measured at 4 m, 5.5 m and 7 m inlet head.

## Specific speed

Using Equation 2.1 the specific speed was calculated as follows:

$$\Omega_s = \frac{\Omega Q^{1/2}}{(gH)^{3/4}} = 0.60 \text{ rad} \quad (4.8)$$

Using the corresponding specific-speed graph, refer to Figure 4.7, the specific speed of the 3I turbine lies within the range of the Francis turbine (refer to Figure 4.2.2).

## Self regulating capacity

The operating conditions set by 3I at installation, are as follows:

- Install the 3I turbine,

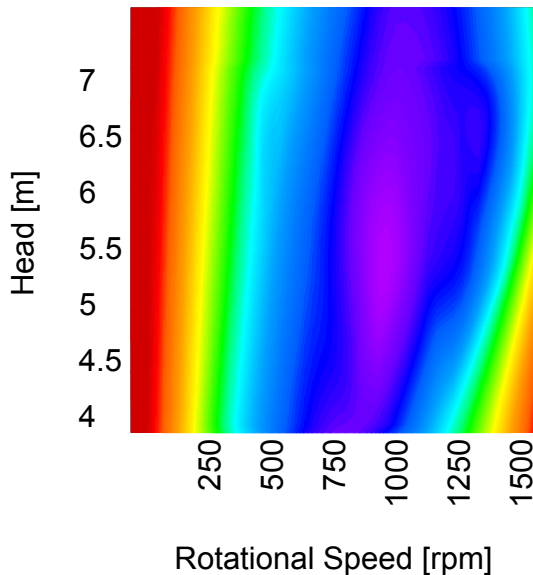


**Figure 4.6.:** Efficiency hill contour plot.

- Measure the maximum rotational speed of the device at no-load condition (runoff speed),
- Design a transmission ratio with the turbine rotating at 75% of its runoff speed; this setting corresponds to operation on the back side of the power curve.

Consider a hypothetical case of a 3I turbine installation whereby the available head pressure is of the order of 5.5 m, the draft tube is submerged in water, and where the power curve equivalent to that shown in Figure 4.8. Moreover, the operation point would be 75% of the runoff speed (according to 3I's operation conditions this equals 1185 rpm). Suppose next that a commonly available 4 pole synchronous generator would be used (a synchronous generator with an automatic voltage regulator (AVR) is highly recommended). This would then imply that the rotational speed of the generator would have to be 1800 rpm. Such a condition could be achieved with a transmission ratio of  $1800 \text{ rpm} / 1185 \text{ rpm} \approx 1.5$ . One of the disadvantages of the off-the-shelf synchronous generators is however, that the maximum safe speed ratio is often unknown. This is, among other reasons, why a larger capacity synchronous generator would be used for these conditions (usually upto 60% larger).

For a micro-hydro system where there are no transformers or induction motors, i.e. where there are only lighting (incandescent or fluorescent lamps), heating and universal (commutator) motor loads, the voltage limits of +7% to -10% and the frequency limits of +10% to -5% of the rated value are recommended (Harvey et al., 2013). This implies that the generator would have to be regulated between  $12057 \text{ Hz} / 4 = 1710 \text{ rpm}$  to  $12066 \text{ Hz} / 4 = 1980 \text{ rpm}$  and that the turbine would have to auto regulate between  $1710 \text{ rpm} / 1.5 = 1140 \text{ rpm}$  to  $1980 \text{ rpm} / 1.5 = 1320 \text{ rpm}$ . The self regulating capacity in terms of rotational speed could then

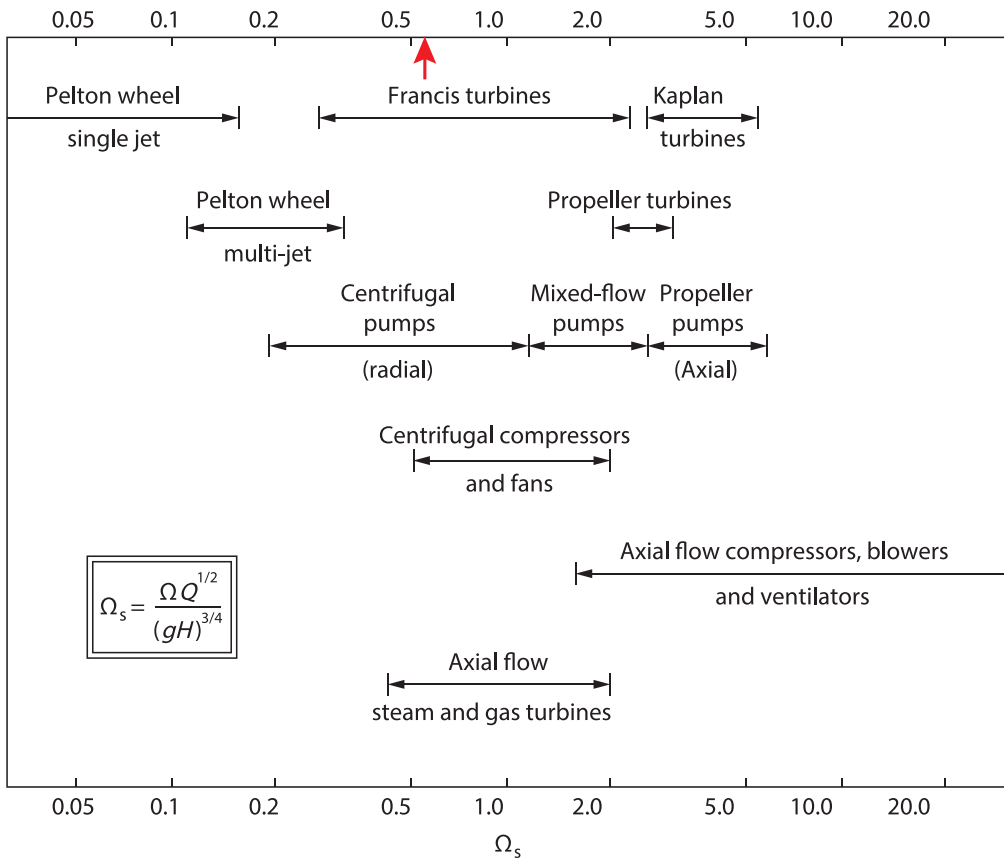


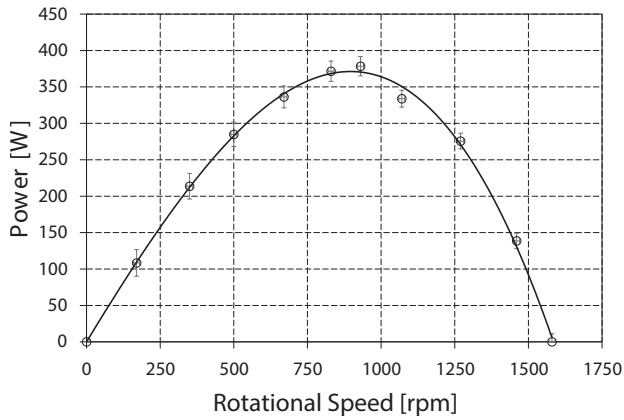
**Figure 4.7.: Range of Specific Speeds for Various Types of Turbomachinery (Dixon and Hall, 2010).**

The red arrow indicates the calculated specific speed of the 3I turbine.

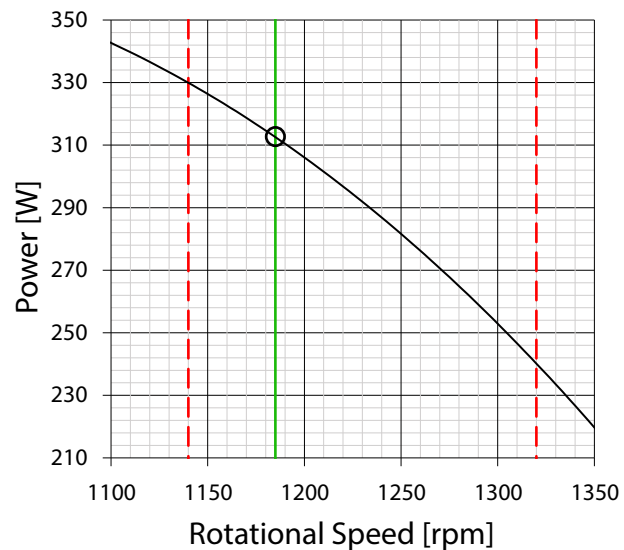
be calculated by:  $(f_{max} - f_{min})/f^*100\% \approx 15\%$ . And The self regulating capacity in terms of power could then be calculated by:  $(P_{max} - P_{min})/P^*100\% \approx 30\%$ .

Figure 4.9 shows a view of Figure 4.8 zoomed in on the operation point and the ranges calculated above.

Although the self-regulating capacity is only -23.8% to +4.8% in terms of shaft power output, the turbine displays a stable operating condition due to the naturally occurring negative feedback loop discussed in Section 2 without any mechanical or electronic control system, therefore, operations under said interval is less expensive and less prone to catastrophic failure.



**Figure 4.8.:** Power curve at 5.5 m head.



**Figure 4.9.:** Power curve zoomed in on the operation point and the regulation ranges.

The circle represents the operation point, and the red dashed lines are the lower and upper frequency limits for the hypothetical case mentioned above.



# Part II

---

Numerical Analysis



# 5

## Steady state numerical flow analysis of the pico hydro turbine under study at a single operating point



*A little misunderstanding?*

*Galileo and the Pope had a little misunderstanding...*

— Sheldon Cooper, B.S., M.S., M.A., Ph.D., Sc.D.  
(The Big Bang Theory)

Fluid flows are governed by a system of Partial Differential and Algebraic Equations (PDAE's) which represent, on the one hand, the mass-, momentum- and energy balance equations, and on the other hand constitutive equations. These flow fields can take complex forms, which is especially the case in turbo machines (Ferziger and Peri, 2002).

In order to theoretically determine the characteristics of a hydro turbine, the behavior of the fluid medium within the turbine, given a set of boundary conditions, must be computed. Due to its complex nature, a numerical software package is a necessity.

Computational Fluid Dynamics (CFD) is an algebraic methodology that replaces PDAE's with a set of algebraic equations which can be solved simultaneously using computers. The accuracy of this method strongly depends on the input data, the mathematical model, the numerical scheme, the grid size and the available computing power (Ferziger and Peri, 2002). Having said that, CFD cannot replace experimental measurements completely, but it does reduce the overall cost of the experiment (Turkowski and Szuflenski, 2013). By applying the CFD techniques on the pico hydro turbine manufactured by 3I, the specific locations of losses can be determined through analysis of the streamline patterns. In principle the losses can also be quantified using rigorous thermodynamics. The tool used to model the turbine and to solve the associated

Speed	Flow Rate	Power	Outlet Pressure	Efficiency	Head (m)
930 rpm	15.249 m <sup>3</sup> · s	378.51 W	99657.87 Pa	46.10	5.5 m

**Table 5.1.:** Experimentally measured data at BEP.

mathematical set of equations for the flow field analyses is ANSYS CFX, in short ANSYS. This software package was selected solely because the authors have experience with the program and therefore they have more control over the setup of the simulation. The pre-processing was done using ANSYS server programs of which in-depth specification will be given further in this document. The simulation was performed at a single steady state operating point of which the data were measured experimentally and given in Table 5.1.

The procedure to setup the simulation involves the following items (ANSYS, 2012f) (Kessler, 2011):

1. Creating the geometry,
2. Generating the mesh for the fluid region,
3. Specifying a set of input data encompassing: (1) the machine type, (2) the reference axis, and with respect to that, (3) the rotating and stationary domain, (4) the topology information, (5) the fluid information, i.e., relevant input data for the computation of local fluid properties, (6) the analysis type, i.e., either steady state or transient, (7) the turbulence and heat transfer model, (8) the boundary conditions, (9) the solver settings, (10) the domain interfaces,
4. Solving the mathematical system of equations,
5. Post processing of the results.

### 5.0.3 Creating the Geometry

Because there was no available design drawing of the turbine under scrutiny, the geometry had to be determined using other means. More specifically the following set of actions was taken: Firstly, the turbine was taken apart completely. The axis of the rotor was taken as reference axis, whereafter the intersection between this axis and the cross-section plane at the outlet was set as the origin. From thereon it was possible to create a fictitious Cartesian coordinate system. Secondly, the turbine volute was measured with a vernier caliper. With this instrument the position of multiple points on the turbine volute were determined, using said origin as the reference. These points were subsequently drawn onto a coordinate system within SolidWorks, which reflects the fictitious Cartesian coordinate system. By connecting these points through splines, closed curves were created. These curves were then lofted together, forming the volute casing. Using this method the accuracy of the geometry mainly depends on the resolution of the measured points. If the geometry in SolidWorks is compared to that of the actual object, the difference is at most of the order of a millimeter.

Thirdly, the turbine rotor had to be drawn, but considering the complexity of the rotor geometry, another approach was taken. To measure the curvatures of the blade vanes a mold of thermoplastic adhesive was made of the rotor fluid passages. Before inserting the mold, the fluid passages were lubricated with oil to prevent adhesive binding between the mold and rotor. Next the thermoplastic adhesive was melted with an electric hot glue gun into the fluid passage creating the mold. This can be seen in Figure 5.1.

After the mold was extracted from the rotor, curves were drawn in the stream-wise direction on the mold (Figure 5.1b), after which these could be measured with a self-made profile gauge. The curves were then plotted onto millimeter paper as shown in Figure 5.3a. This procedure was repeated for five layers along the height of the vane. The curves are then drawn in SolidWorks where they are lofted together (Figure 5.3c). It is worth mentioning that only one blade was plotted and then equally arrayed around the hub, summing a total of twelve blades. The physical rotor, in contrast, is hand fabricated and exhibits noticeable deviations in mutual blade spacing and blade curving. It must be kept in mind that this discrepancy has an effect when validating



(a)Turbine rotor passage filled with thermo-plastic adhesive. (b)Mold after extraction from the turbine rotor.

**Figure 5.1.:** Thermoplastic adhesive between the rotor vanes.

the simulation results with experimental data, necessitating prudence.



(a)Measuring the curvature of the mold. (b)Measured curve on the profile gauge.

**Figure 5.2.:** Curve measurement using a profile gauge.

Finally, the remaining parts such as the hub, shaft, bearings, seals, etc. are symmetric geometries with respect to the axis of rotation and they are comparatively easy to draw. Dimensions were taken with a vernier caliper. Following the steps above resulted in the geometry displayed in Figure 5.4.

#### 5.0.4 Creating the Simulation Geometry

Starting from Figure 5.4, which is a replica of the physical model, i.e., the boundary of the simulation model, the geometry needed for the numerical analyses is created. This geometry must only represent the fluid domain, as it is in this domain that one is interested in the flow

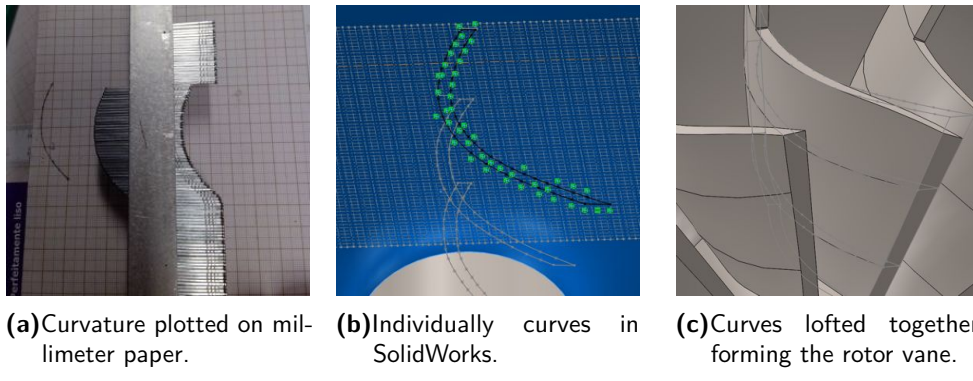


**Figure 5.3.:** Plotting of the curvatures.



**Figure 5.4.:** Drawing of the hydro turbine under investigation.

field. To create this geometry, the starting model is “filled”, after which this filled body is extracted from the whole. The filled body then represents the simulation domain. Figure 5.5 gives a preview of the geometry versus the extracted simulation domain. In hindsight it proved to be difficult for the rotor geometry to be imported into ANSYS, considering the need to define the topology of the rotor. It was therefore decided to develop the fluid domain in ANSYS itself. Since this problem was not encountered for the volute because of the absence of inlet guide vanes (IGV's), the fluid domain was imported from SolidWorks using ANSYS' built-in wizard.

### 5.0.5 Creating the Turbine Rotor in ANSYS BladeGen

ANSYS uses the server program BladeGen and it is especially developed for creating the geometry of rotating machinery. This program provides an essential link between blade design and advanced meshing programs. The tools used by BladeGen are industry specified and universal among blade designers (ANSYS, 2010).

When creating a design in BladeGen, first the type of rotating machine must be specified, which

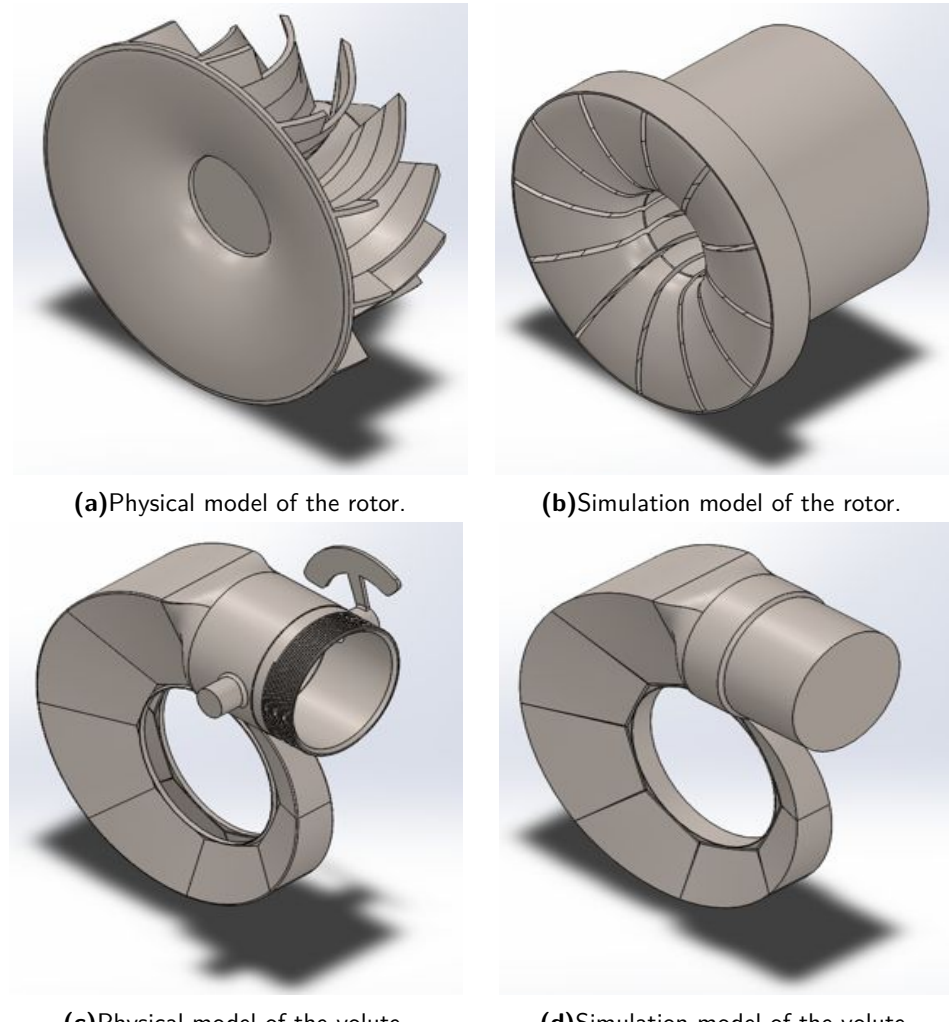


**Figure 5.5.:** Physical geometry of the turbine versus the flow field simulation domain.

for this case is a radial turbine. Next, the hub en shroud contours must be defined in BladeGen, see Figure 5.6; therein the coordinates of the contour lines are indicated with open circle symbols. The streamlines seen in this figure are automatically created in BladeGen.

A noteworthy observation is that the streamlines do not exhibit a smooth transition from the leading edge (LE) to the trailing edge (TE). Solely from this trend it can a priori be stated that this non-smooth transition penalizes the turbine efficiency (ANSYS, 2010).

The fluid regions at the LE and TE of Figure 5.6 are also automatically created by BladeGen, but can be modified to the user's preferences. ANSYS recognizes the fluid region at the LE as a transition region between the stator and rotor vanes. Due to the absence of IGV's, it is difficult to assess the region's size, as one can only define this through examination of the solution simulation, that is to say after suitable post-processing. If the solution proves the region to be of incorrect size, the region must be modified; this process requires iteration.

Hereafter the normal layer thickness of the blade must be specified. For the investigated turbine the blade thickness is constant and equal to 2 mm.

The last step and probably the most difficult one is to define the curvature of the rotor vanes. The curves are defined by manually inserted points which are then automatically connected

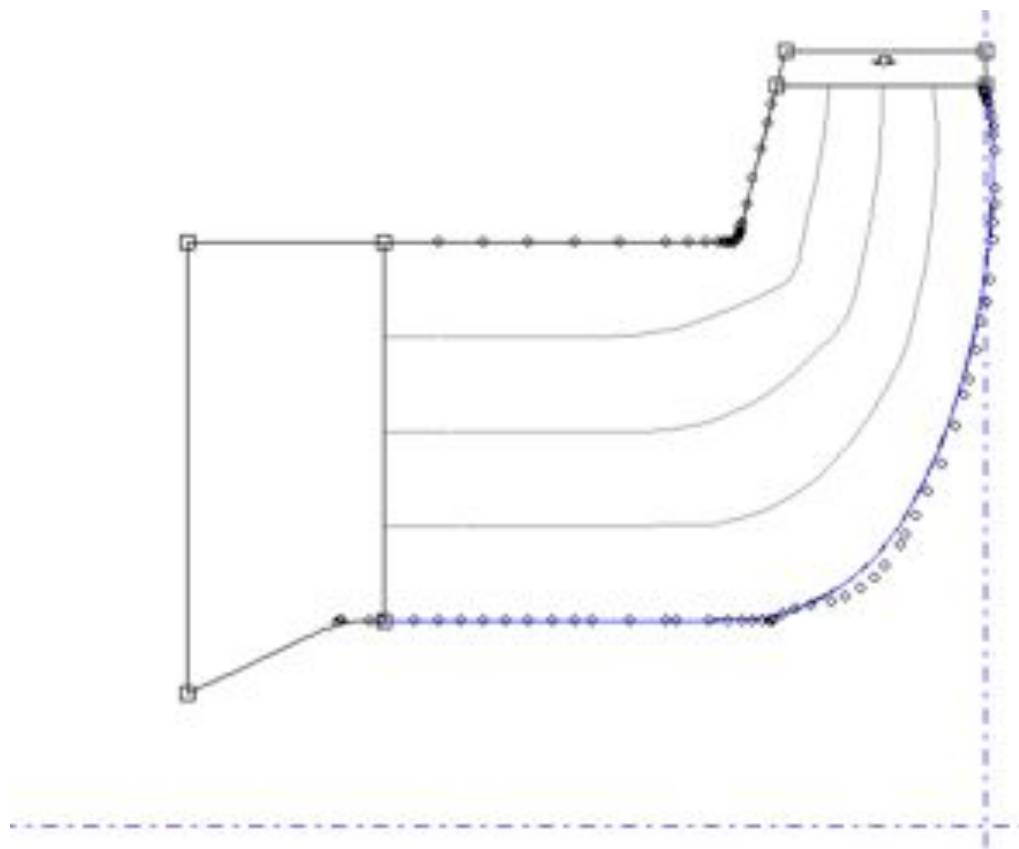


**Figure 5.6.:** 2D projection of the hub and shroud contours.

through splines with the aid of BladeGen. These points are measured from the SolidWorks drawing and must be imported as cylindrical coordinates  $(\rho, \varphi, z)$  into BladeGen.

There are two ways to divine the points on the curve viz., either in the span wise or in stream wise direction. For this case the stream wise direction was taken, since the radial distance ( $\rho$ ) from the rotation axis to the streamlines was already generated when the hub and shroud contours were defined. The azimuth angles ( $\varphi$ ) were calculated from Equation 5.1 and the  $z$  coordinates were chosen randomly.

$$\varphi = \begin{cases} 0, & \text{if } x = 0 \text{ and } y = 0 \\ \arcsin\left(\frac{y}{\rho}\right), & \text{if } x \geq 0 \\ -\arcsin\left(\frac{y}{\rho}\right) + \pi, & \text{if } x < 0 \end{cases} \quad (5.1)$$

It is worth mentioning that only the hub and shroud curves were used to generate the vane's geometry. The radial distance ( $\rho$ ), from the intermediate streamlines were difficult to assess and thus, because these streamlines had in hindsight/arguably a rather in-significant contribution to the resolution of the vane's geometry, they were left out.

## 5.1 Creating the Rotor Mesh

The subsequent step to setup the simulation is the mesh creation. For this purpose the stationary volute as well as the moving rotor are meshed with respectively ANSYS ICEM CFD and ANSYS TurboGrid which are ANSYS server programs.

Figure 5.7 gives a mind-map of the setup of the simulation for subsequent numerical computations using ANSYS CFX.



**Figure 5.7.:** Project schematics of the simulation of the Indalma turbine.

### 5.1.1 Meshing the Rotor Using TurboGrid

ANSYS TurboGrid is a software especially designed to create meshes for turbo machinery. By transferring the geometry data from ANSYS BladeGen to ANSYS TurboGrid, the machine data is automatically generated, meaning that TurboGrid recognizes the location and structure of the hub, shroud, blade, low- and high periodic,<sup>1</sup> inlet and outlet (ANSYS, 2012e).

The remaining steps to establish the mesh are:

- Defining the topology,
- Reviewing the mesh data settings,

<sup>1</sup>The low- and high periodic are fictitious interfaces between two adjacent fluid passages.

- Analyzing the mesh,
- Saving the mesh,
- After post-processing it may be necessary to refine the mesh.

### 5.1.2 Defining the Topology

A precursor to meshing is the placement of the topology. ANSYS offers two features for the latter namely an automatic placement (hereinafter referred to as ATM Optimized) or a traditional one obtained via the placements of control points. The ATM Optimized feature enables one to control the global mesh size as well as the mesh size at and near the boundary. This feature is generally easier to use than the traditional one which requires a sufficient amount of CFD knowledge by the user. What is more is that the ATM Optimized feature tends to yield a better mesh contrary to the traditional approach (ANSYS, 2012e). For this simulation the ATM Optimized feature was used. This feature provides a list of topology families of which the user can manually choose one best suited to the machinery under scrutiny. Worth mentioning is that TurboGrid has already filtered this list, thus reducing the chance of a faulty topology. For this simulation the Single Cutoff Cutoff method was used. The topology can then be generated, after which the mesh data settings can be reviewed by the user (ANSYS, 2012e).

### 5.1.3 Reviewing the Mesh Data Settings

When using the ATM Optimized feature the default mesh and base mesh dimensions are automatically computed. All the mesh dimensions have edge refinement factors which are multiplied by the base mesh dimensions and global size factors to determine the final mesh size (ANSYS, 2012e). For the turbine herein the boundary layer offset was set to grow proportional to the mesh size, which controls the number of elements across the boundary layer in proportion to a factor ratio. If chosen otherwise either an edge refinement factor or a first element factor is to be specified. The element size near the wall is calculated with the aid of an initially guessed Reynolds number of  $1 \cdot 10^6$ , which corresponds with a  $y^+$  of approximately 183 within the fluid passage. Remark that no exact study has been done to determine the Reynolds number of the flow through the rotor passage and thus the height of the turbulent boundary layer is unknown (Pasquale, 2014).

### 5.1.4 Analyzing the Mesh

ANSYS TurboGrid has a built in mesh analyzer that examines the mesh on the following variables:

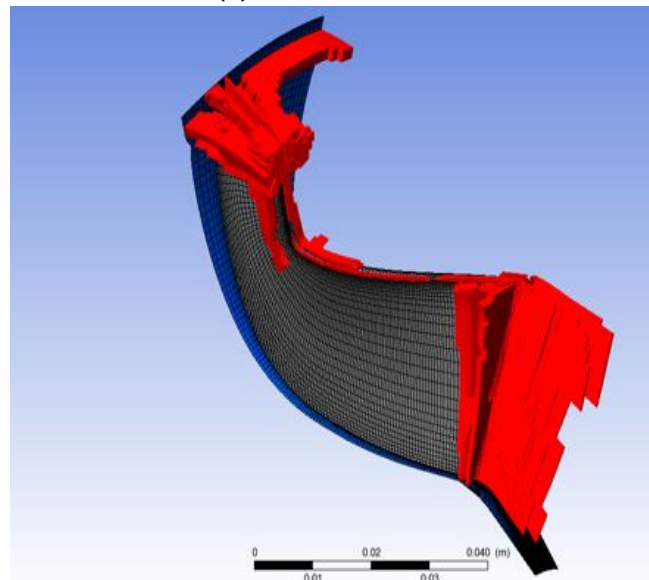
- The face angle,
- The element volume ratio (with respect to a node),
- The element volume size,

- The edge length ratio (with respect to a node),
- The connectivity number (with respect to a node).

The analysis result of the mesh, created as described in the previous sections, is displayed in Figure 5.8a. The limit of the maximum element volume ratio and the maximum edge length ratio were set to respectively 2 and 100, yielding a total of roughly 3.6% of the elements to fall outside of this limit. Figure 5.8b displays the regions where these elements are concentrated. With the exception of extremely dense meshes it is normal that mesh elements near the wall have very high length and volume ratios (ANSYS, 2012a).



(a) Mesh statistics of the rotor mesh.



(b) Concentrated error regions indicated in red.

**Figure 5.8.:** Mesh statistics of a single fluid passage in the rotor.

## 5.2 Creating the Volute Mesh

The stationary volute was meshed using ANSYS ICEM CFD. This is a server program of ANSYS specifically designed to mesh complex geometries and uses advanced mesh diagnostics and interactive and automated mesh editing (ANSYS, 2012b).

The geometry wherfrom the fluid domain can be inferred, is imported from SolidWorks. Next, the inlet, outlet and fluid domain are defined. The mesh type chosen for the fluid domain in the volute is a tetra/prism mesh. The tetra mesh is a “tetrahedral/pyramid” mesh type used for 3D meshes of which the geometry is unstructured (complex), a criteria, that fits the volute casing. The tetra mesh however, is not efficient to accurately capture the boundary effects, this is where the prism mesh comes in (ANSYS, 2012b).

The spacing of the prism layers enables the solver to capture the  $y^+$  region (related to the turbulent boundary layer). The solver performs calculations between nodes or elements, where in relation to volume meshes, a prism mesh generates more elements perpendicular to the surface. This is an efficient way to achieve better resolution (i.e., more calculations per unit distance) of the solution normal to the surface, without increasing the number of elements along the surface. The prism mesh also gives a quicker and more accurate solution than can be achieved with a very fine tetra mesh (ANSYS, 2012d).

The remaining steps to setup the mesh are:

- Generating the Octree Mesh,
- Generating the Delaunay Mesh,
- Creating the Prism layer,
- Saving the mesh.

With respect to the first two items hereinabove the following should be stated: the aim is to create a Delaunay mesh starting from a Octree surface mesh (details are given in due course) (Ansys, 2010a).

### 5.2.1 Generating the Octree Mesh

Before generating the Octree mesh, first the Global Mesh Setup must be edited (ANSYS, 2012d). Here the global element seed size (that is the maximum element size) is set to 2 mm. This size was chosen based on an estimated hydraulic diameter of the smallest passage (ANSYS, 2012c). ANSYS recommends that the value for the global element seed size equals a power of two. If chosen otherwise ANSYS will, in most cases, automatically correct the input value to satisfy the above mentioned recommendation. The user cannot control the settings of this feature (ANSYS, 2012b).

After the Global Mesh Setup is edited, the volume mesh is computed using the Octree method. This mesh, as can be seen from an example displayed in Figure 5.9, shows a relatively large transitions from the surface to the volume. Furthermore, from a CFD point of view, this mesh is not desirable because the structure forms a consistent pattern, which fails to represent the

physical model. To smoothen these surface-to-volume transitions the mesh is further calculated using a Delaunay mesh method which is described further (Ansys, 2010b).

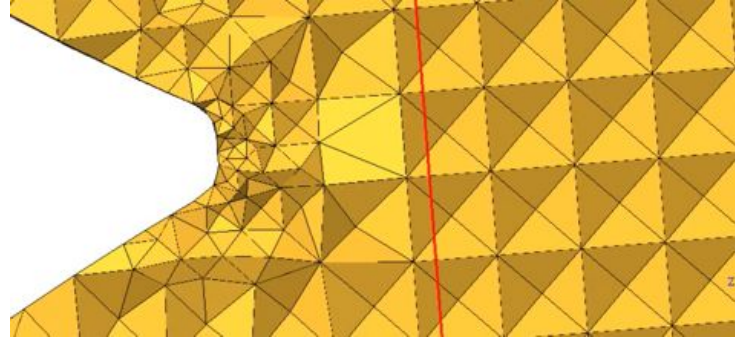


**Figure 5.9.:** Octree mesh generation.

### 5.2.2 Generating the Delaunay Mesh

In mathematics and planimetry, a Delaunay triangulation for a set of points  $P$  in a plane is a triangulation  $DT(P)$  such that no point in  $P$  is inside the circumcircle of any triangle in  $DT(P)$ . Delaunay triangulations maximize the minimum angle of all the angles of the triangles in the triangulation; they tend to avoid skinny triangles (Rebay, 1993). Because the Delaunay mesh grows from the surface mesh, the Octree volume mesh must first be deleted, whereafter the Delaunay mesh can be computed (Ansys, 2010b). Figure 5.10 displays a Delaunay mesh that was grown from the surface out. Compared to the Octree mesh, this mesh has much smoother transitions and a less structured volume mesh.

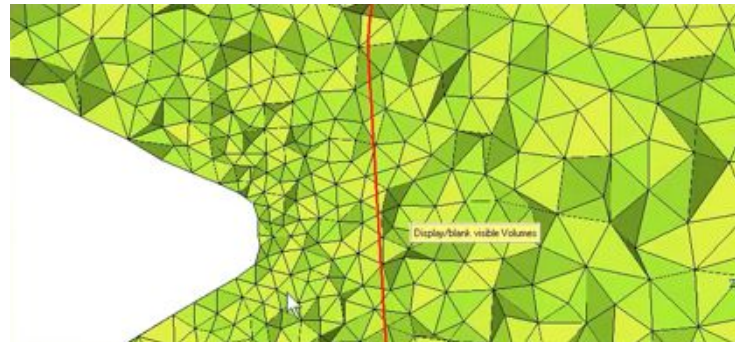


**Figure 5.10.:** Delaunay mesh generation.

### 5.2.3 Creating the Prism layer

Because the Reynolds number in the stationary volute is unknown, the behavior of the fluid within the turbulent boundary layer is unknown. It is because of this, that the Prism Meshing Parameters are set to their default values, meaning that the mesh was set to grow exponentially and that the number of layers was set to 5 (Pasquale, 2014). Note that only at and near the

walls a prism mesh is needed. For this reason the inlet and outlet of the stationary volute are left according to the Delaunay mesh. Figure 5.11 displays the tetra/prism mesh.

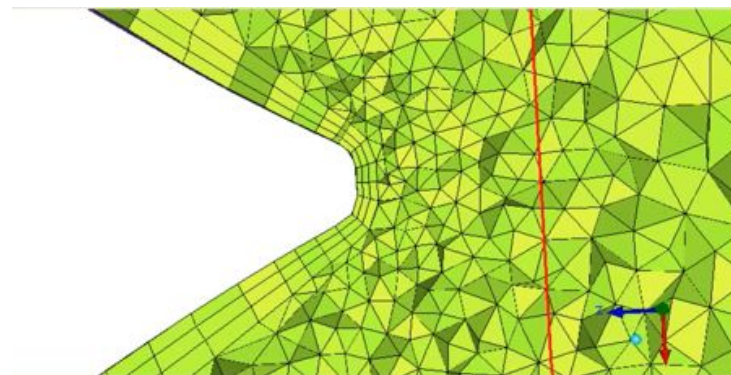


Figure 5.11.: Tetra/prism mesh generation.

## 5.3 ANSYS Turbo Pre: Preparation for Numerical Computation

ANSYS CFX has a built in mode that is specialized in preparing turbo machinery simulations, such as compressors, fans and turbines in a “simple” manner. When using this mode the rotor and stator domain can be defined, whereafter the boundary conditions and interfaces can be edited. Turbo mode is a wizard which guides the user through the pre-analysis process (ANSYS, 2012f). For this reason the preparation of the simulation is documented hereunder, in a stepwise manner.

**Step 1 Basic Settings.** For the machine type “Radial Turbine” was chosen from a drop down list, the rotation axis was set along the Z axis and the analysis type was set to be steady state.

**Step 2 Component definition.** In this step the stationary and rotating domain were set. In case of the rotor the domain was set to be rotating and as the simulation is steady state at a single operating point, the rate of rotation was set to 930 rpm. This value corresponds with the experimental data, taken at BEP. For the case of the volute, the domain is set to be stationary.

**Step 3 Physics Definition.** This step can be subdivided into 3 (three) items, namely:

- Fluid type: the fluid medium is water.

- Model data: the turbulence model chosen for this simulation is the Shear Stress Transport (SST) model. This model best represents turbo machinery, a claim supported by many CFD practitioners (see e.g. cfd-online.com). To verify this claim, the second turbulence model option,  $k-\epsilon$ , was applied, which indeed failed to converge.
- Inflow/outflow boundary templates: for the inflow a mass flow rate of 14 l/s was set at a static outlet pressure of 1 atm.
- Physical interface: the physical interface was set to “stage” as the default type.

**Step 4 Boundary and interface definition.** In this step the boundary and interface regions were applied to the file data (rotor and volute mesh).

Relevant details of the simulation setup are documented in Appendix C.



# 6

## Numerical Results

### Results

“ Ah— memory impairment.  
The free prize at the bottom of every vodka bottle.

In the present  
— Sheldon Cooper, B.S., M.S., M.A., Ph.D., Sc.D.  
(The Big Bang Theory)

study solely the BEP was used as operating point, stating that at this point the fluid within the turbine reaches its maximum momentum transfer per unit power and it can thus be assumed that the streamlines resulting from this simulation give a valid representation as to where the regions of losses are located. The velocity profile at the inlet of casing is uniform and evenly distributed. From this point on, the stream gradually transforms into a vortex-free flow as it advances towards the LE of the rotor, as shown in Figure 6.1.

The approximately smooth and uniform pressure distribution in Figure 6.1 around the rotor, as

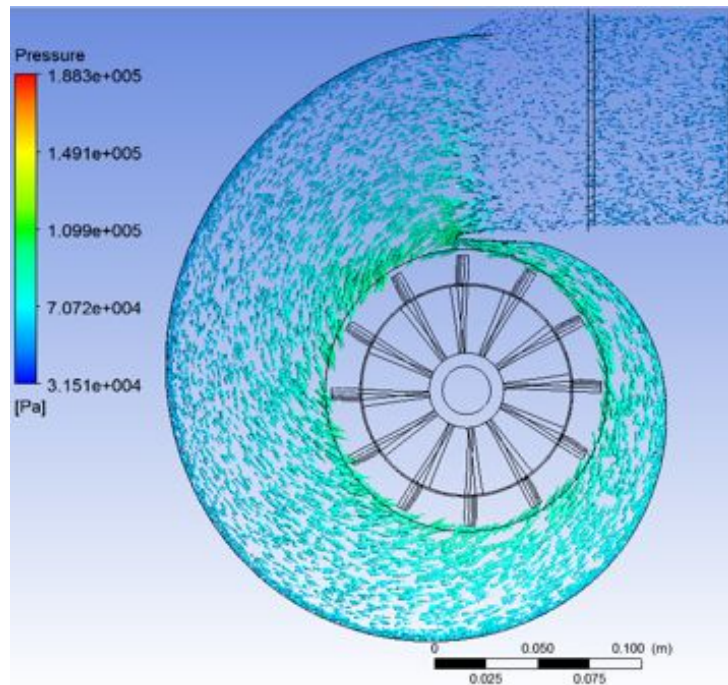
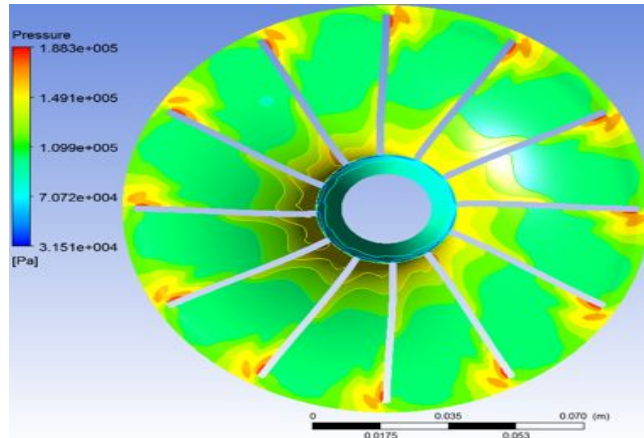


**Figure 6.1.:** Velocity vector field and pressure distribution of the volute casing.

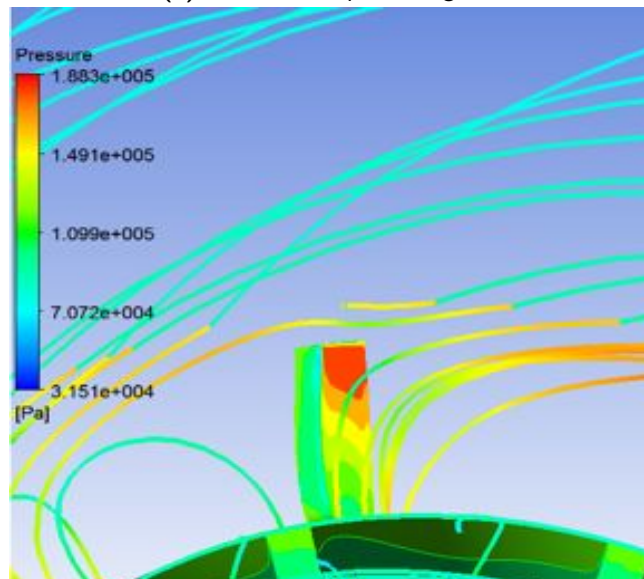
observed in a stationary reference frame, yields a uniform velocity vector field and therefor the

flow exiting the volute into the rotor is uniform all around. Conversely, for the rotor there are clear locations where there is a higher pressure gradient than elsewhere, see Figure 6.2a. From the viewpoint of a rotating reference frame, this is caused by a mismatch between the angle of attack and the rotor blade angle, as is elucidated in Figure 6.2b

As Figure 6.3a and 6.3b illustrate the pressure distribution over respectively the pressure- and



(a) Pressure field plotted against the rotor hub.

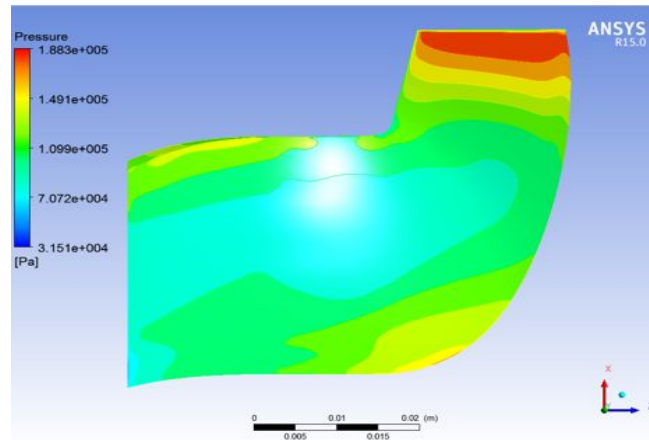


(b) Flow field collision at LE of a rotor vane.

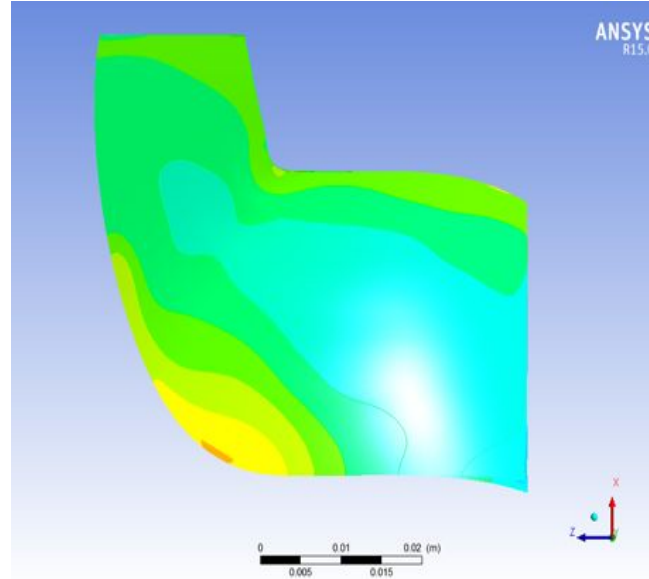
**Figure 6.2.: Simulation results of the rotor region.**

suction side of rotor vane is not uniform. This inconsistency is more pronounced at the LE of pressure side. Considering an ideal rotor vane, uniformity of the pressure distribution is desired, since the pressure contour indirectly influences the delivered torque. Given the fact that for this turbine the pressure distribution along the rotor blade vane is non-uniform, implies that a fraction of the blade is ultimately not used for power generation. This case is made more obvious with the aid of Figure 6.4 where the pressure difference between the pressure- and suction side are illustrated. Figure 6.4 is a pressure sample plot created within ANSYS Post. The initially lower dotted-line represents the pressure curve of the suction side, whereas the upper dotted-line represents that of the pressure side. Analyzing this plot shows that only about the first 30%

of the blade (With respect to the streamline at a span of 0.5) is suitably utilized, whereas the latter part is not. The condition is exacerbated, since the subsequent 30% of the blade results in a power loss, as can be inferred from the crossing of the dotted-lines cross each other. This can be explained due to detachment of the boundary layer as a consequence of flow vortices. Furthermore, the static pressure at the TE is less than the atmospheric pressure and as a result thereof the water fills up all the passages of the rotor (Figure 6.5).



(a) Pressure side of a single rotor vane.



(b) Suction side of a single rotor vane.

**Figure 6.3.:** Meridional view of the rotor vane.

Blade Loading Chart

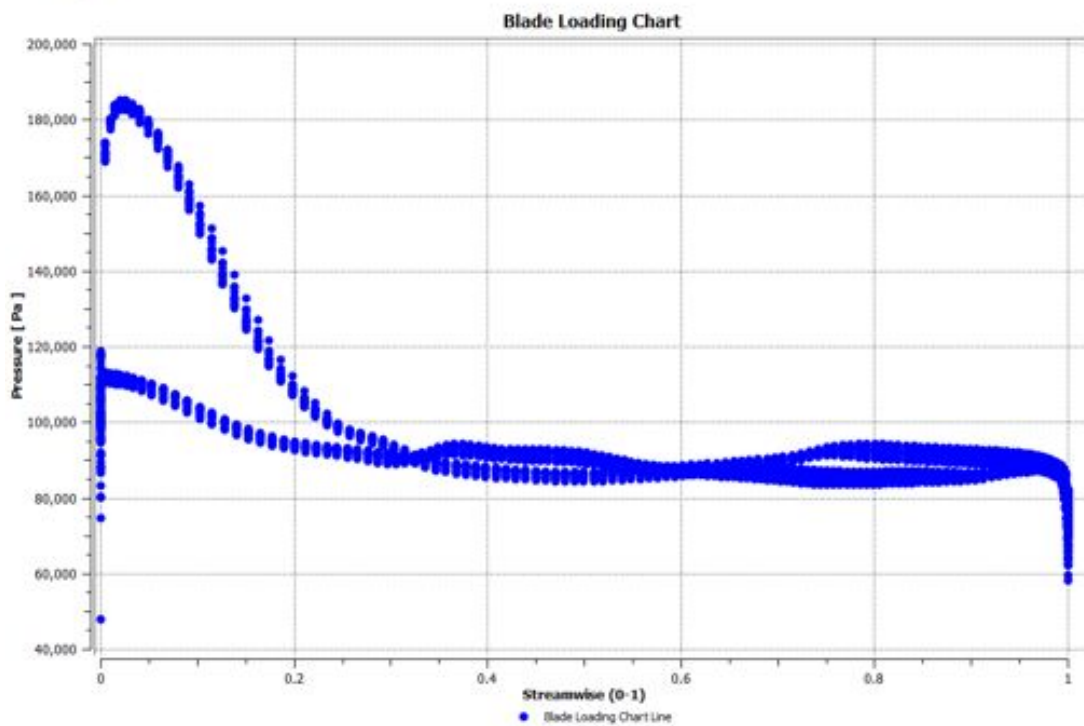


Figure 6.4.: Blade loading chart.

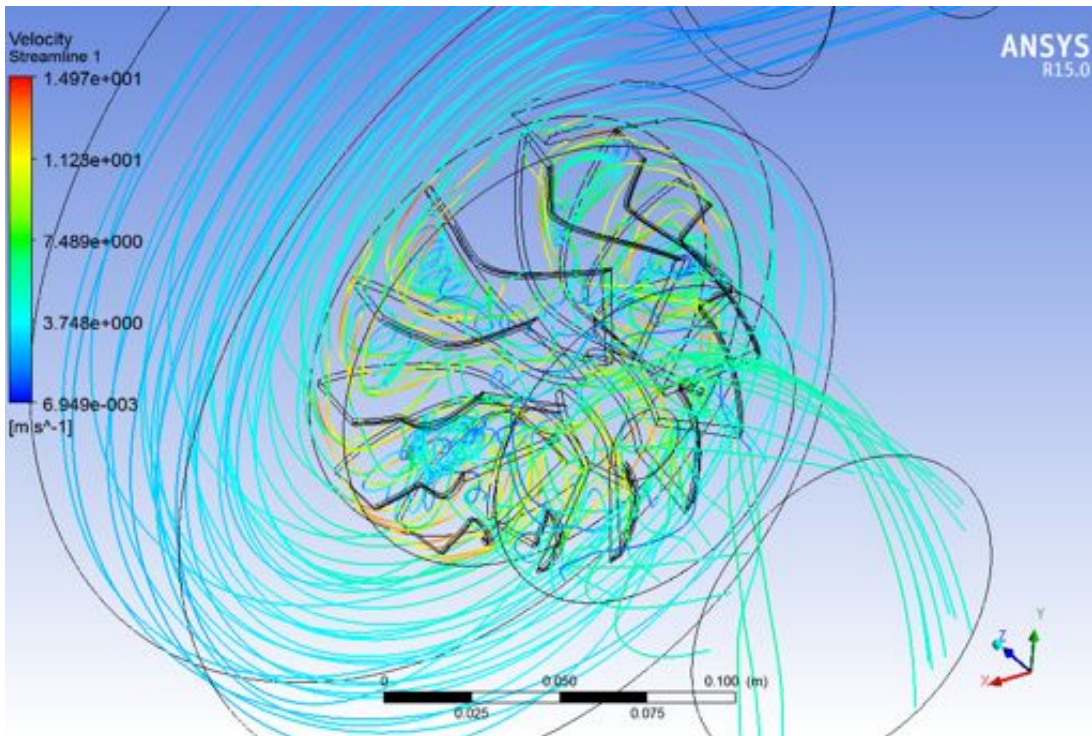


Figure 6.5.: Vortex field within the turbine rotor.

---

## Conclusions & Recommendations



# Conclusions

**“** I got an idea, an idea so smart my head would explode if I even began to know what I was talking about.

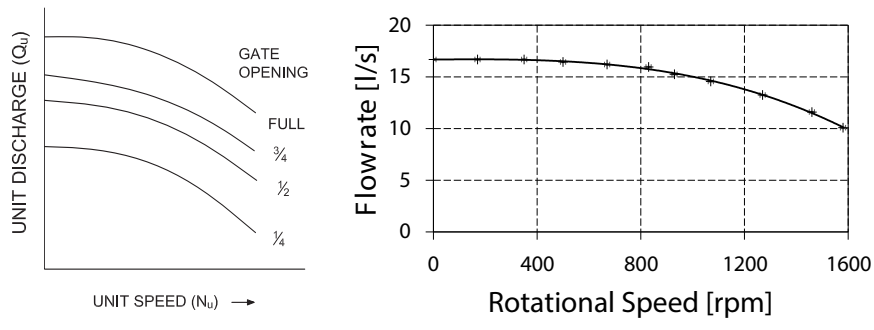
— Peter Griffin  
(Family Guy)

## 7.1 Characteristics of the Indalma turbine

In summary, this work documents the experimentally acquired performance characteristics of a 3I pico hydro turbine, and starting from those results, a CFD simulation has been performed. The aim of conducted simulations was to qualitatively, and to a certain degree quantitatively, assess the occurring flow losses which result in performance deterioration. Simulation results have been validated for a single operating condition with the obtained experimental data.

Recall that the aim of the experimental work was to: (1) classify the turbine using the performance curves and the specific speed, and (2) assess the self-regulating capacity relevant for deploying this system in the field.

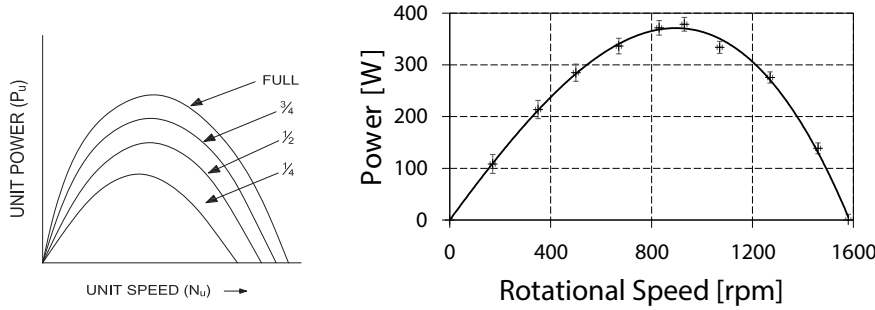
Comparing the characteristics of the Francis turbine with the experimentally obtained characteristics of the 3I turbine, one can argue that the initial hypothesis, formulated in Section 1, is validated. That is to say that indeed the 3I turbine is of the Francis type. This finding is confirmed with the specific speed according to Equation 2.1 and Figure 4.7. Additionally, it has been found from the experiments that the maximum power output at the shaft of the 3I turbine under investigation is of the order of 530 W at  $\sim 1050$  rpm with a total efficiency of approximately 44%.



(a) Francis turbine.

(b) Indalma turbine.

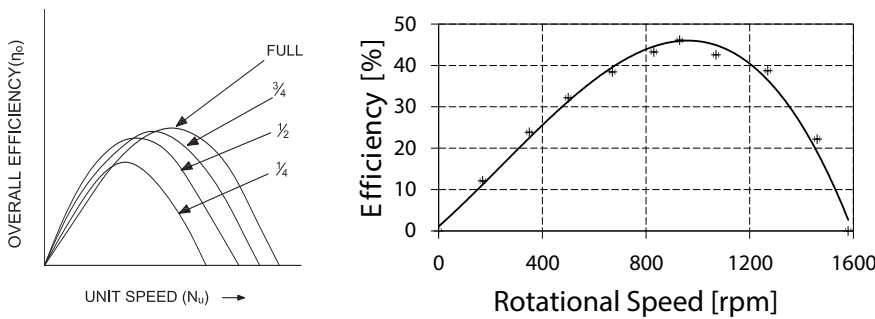
Figure 7.1.: Flow curves at constant head.



(a)Francis turbine.

(b)Indalma turbine.

**Figure 7.2.:** Power curves at constant head.



(a)Francis turbine.

(b)Indalma turbine.

**Figure 7.3.:** Efficiency curves at constant head.

Notice that in Figure 7.2 the peak in the power curve of the Francis turbine is more to the left of the center, while the peak of the power curve of the Indalma turbine is more to the right of the center.

Given that the available inlet head is 5.5 m the experimentally obtained power performance curves indicate that the scrutinized 3l turbine indeed has self-regulating capacity under the provision that the rotational speed is greater than about 1000 rpm. If this turbine would be indeed deployed in the field then at the shaft: the nominal rotation speed would be around 1180 rpm, the power output would be about 310 W and the efficiency would be of the order of 46%.

## 7.2 Regions of losses

Presented within this study is a preliminary CFD analysis of a 3l turbine, allowing the authors to quickly and efficiently determine the flow behavior within the turbine, and thus identifying the regions of losses. As can be concluded or rather confirmed, is that the efficiency of this turbine,

proves to be rather low.<sup>1</sup> The cause hereof is a summation of errors/deviations of the turbine's geometry. Starting with the turbine volute, which proves to have a fairly smooth scroll casing wherein losses are negligible, due to the absence of IGV within the volute, there is a mismatch of the streamlines at the LE, resulting in high losses at the rotor inlet. Secondly, the streamlines at the shroud do not exhibit a smooth transition from LE to TE, resulting in a sudden deflection of the streamlines and therefore an unnecessary power loss. Finally, it can be concluded that due to the incorrect design of the rotor vane, boundary layer detachment is observed at approximately 30% along the streamline direction, meaning that up to 70% of the blade area is unused so to say.

---

<sup>1</sup>Typically efficiencies of such turbines can reach beyond the order of 70% as opposed to the value of roughly 46% for this device Mendes and Oliveira, 2013.



# 8

## Recommendations

“

*I've eaten things that didn't complain this much.*

— **Diego**  
(Ice Age)

Although the self regulating capacity has been assessed using procedures 3I applies to conditions in the field, the experimental work has not focused on the dynamics of the turbine and of the balance of plant. Moreover it is worth assessing the influence of the draft tube design on the performance parameters.

Based on the findings within this work, only statements at a single operating point can be made. Nonetheless these results clearly identify the areas of losses. Based on the velocity vector field and overall pressure distribution, the following recommendations can be made (with or without the use of CFD): (1) design and placement of IGV, (2) improvement of the rotor blade design, (3) smoothing of the shroud contour.



# Bibliography

- Ansys (2010a). *Ansys 12.1 (part 1 of 2) icem cfd setup for tetra\_prism meshing of a simple manifold*. Available at: <http://www.youtube.com/watch?v=SdUjpjwUnew>  
Access date: 3-31-2014 (cit. on p. 46).
- Ansys (2010b). *Ansys 12.1 (part 2 of 2) icem cfd setup for tetra\_prism meshing of a simple manifold*. Available at: [http://www.youtube.com/watch?v=C1Yw\\_pYaPGE](http://www.youtube.com/watch?v=C1Yw_pYaPGE)  
Access date: 3-31-2014 (cit. on p. 47).
- ANSYS (2010). *ANSYS CFX-BladeGen Tutorials*. 12.0. ANSYS, Inc. Southpointe, 275 Technology Drive, Canonsburg, PA 15317 (cit. on pp. 40, 41).
- (2012a). *ANSYS CFX Tutorials*. 14.5. ANSYS, Inc. Southpointe, 275 Technology Drive, Canonsburg, PA 15317 (cit. on p. 45).
  - (2012b). *ANSYS ICEM CFD Help Manual*. 14.5. ANSYS, Inc. Southpointe, 275 Technology Drive, Canonsburg, PA 15317 (cit. on p. 46).
- ANSYS (2012c). *ANSYS ICEM CFD Tutorial Manual*. 14.5. ANSYS, Inc. Southpointe, 275 Technology Drive, Canonsburg, PA 15317 (cit. on p. 46).
- ANSYS (2012d). *ANSYS ICEM CFD User Manual*. 14.5. ANSYS, Inc. Southpointe, 275 Technology Drive, Canonsburg, PA 15317 (cit. on p. 46).
- (2012e). *ANSYS TurboGrid Tutorials*. 14.5. ANSYS, Inc. Southpointe, 275 Technology Drive, Canonsburg, PA 15317 (cit. on pp. 43, 44).
  - (2012f). *ANSYS TurboSystem User Guide*. 14.5. ANSYS, Inc. Southpointe, 275 Technology Drive, Canonsburg, PA 15317 (cit. on pp. 38, 48).
- Bansal, R.K. (2007). *Solid and Fluid Mechanics*. Ed. by Smt. Nirmal Bansal. Laxmi Publications (Pvt) Limited (cit. on pp. 8, 10).
- Dixon, S. L. and C. A. Hall (2010). *Fluid Mechanics and Thermodynamics of Turbomachinery*. 6th ed. Elsevier (cit. on pp. 6–8, 32).
- Els, Rudi Henri van, Ramsay Mac Donald, Nigel Sloot, et al. „Auto-regulating behavior of an Indalma hydraulic turbine in microhydropower plant (To be published)“. In: *Centro Nacional de Referência em Pequenas Centrais Hidrelétricas CERPCH* (cit. on p. 2).
- Els, Rudi Henri van, J.N.S. Vianna, and A.C.P. Brasil (2010). „Eletrificação rural em Santarém: contribuição das microcentrais hidrelétricas“. In: *Revista Brasileira de Energia* 16.2, pp. 35–46 (cit. on p. 1).

- Els, Rudi Henri van, J.N.S. Vianna, and A.C.P Brasil Junior (2012). „The Brazilian experience of rural electrification in the Amazon with decentralized generation - The need to change the paradigm from electrification to development“. In: *Renewable & Sustainable Energy Reviews* 16.3, pp. 1450–1461.
- Ferziger, J. H. and M. Peri (2002). *Computational Methods for Fluid Dynamics*. Third. Bertelsmannspringer publishing group (cit. on p. 37).
- Global Hydropower Scenario* (2007). Environmental Resources Group (P) Ltd.
- Harvey, A., A. Brown, P. Hettiarachi, and A. Inversin (2013). *Micro-Hydro Design Manual*. Practical Action Publishing, p. 374 (cit. on pp. 5–12, 28, 31).
- Husain, Zoeb, Mohd Zulkifly Abdullah, and Zainal Alimuddin (2008). *Basic Fluid Mechanics and Hydraulic Machines*. BS Publications (cit. on pp. 2, 5, 24).
- Hydropower* (2013). International Energy Agency.
- Kessler, Martin (2011). *CFD Applied to Turbomachinery*. ESSS (cit. on p. 38).
- Mendes, Rafael Castilho Faria and Taygoara Felamingo de Oliveira (2013). „*METHODOLOGY FOR HYDRAULIC MICROTURBINES TESTING*“. In: *COBEM* 22 (cit. on p. 59).
- Pasquale, David (2014). „Expert advice“ (cit. on pp. 44, 47).
- Raabe, Joachim (1985). *Hydro Power: the design, use, and function of hydromechanical, hydraulic, and electrical equipment*. 1st ed. VDI Verlag (cit. on p. 6).
- Raikar, R.V. (2012). *Laboratory Manual Hydraulics And Hydraulic Machines*. PHI Learning (cit. on p. 11).
- Rebay, S. (1993). „Efficient Unstructured Mesh Generation by Means of Delaunay Triangulation and Bowyer-Watson Algorithm“. In: *Elsevier*. Available at: <http://www.sciencedirect.com/science/article/pii/S0021999183710971> Access date: 5-8-2014 106.1, pp. 125–138 (cit. on p. 47).
- RenewablesFirst. *Renewables First*. Available at: <http://www.renewablesfirst.co.uk/hydro-learning-centre/what-is-the-difference-between-micro-mini-and-small-hydro/> Access date: 11-16-2013 (cit. on p. 6).
- Turkowski, M. and P. Szuflenski (2013). „New Criteria for the Experimental Validation of CFD Simulations“. In: *Elsevier* 34, pp. 1–10 (cit. on p. 37).
- Verlaan, R., V. Ajodhia, J. Balijn, et al. (2008). *Suriname power sector assessment and alternatives for its modernization (ATN/SF-9038-SU) - Preliminary Assessment Report*. Tech. rep. Ministry of Natural Resources of Suriname (cit. on p. 1).
- White, Frank M. (2011). *Fluid Mechanics*. Ed. by Lora Neyens. 7th ed. McGraw-Hill Companies, pp. 734–739 (cit. on p. 24).

# List of Figures

2.1	Range of Specific Speeds for Various Types of Turbomachinery (Dixon and Hall, 2010). . . . .	7
2.2	Pelton wheel. . . . .	8
2.3	Constant head characteristics of a Pelton turbine (Bansal, 2007). . . . .	8
2.4	Kaplan turbine. . . . .	9
2.5	Constant head characteristics of a Kaplan turbine (Bansal, 2007). . . . .	10
2.6	Francis turbine . . . . .	10
2.7	Constant head characteristics of a Francis turbine (Raikar, 2012). . . . .	11
2.8	A method for reducing overspeed risks. . . . .	12
3.1	Schematic overview of the experimental test setup. . . . .	13
3.2	The WEG CFW09 inverter. . . . .	15
3.3	De Prony Brake. . . . .	16
3.4	Rotational speed sensor. . . . .	17
3.5	The V-notch flow measurement instrument. . . . .	17
3.6	Pressure measuring instruments. . . . .	18
3.7	Data Acquisition system diagram. . . . .	18
3.8	CW552 kit DAQ system. . . . .	19
3.9	Front view of the Arduino Uno. . . . .	20
3.10	Arduino shield for DAQ. . . . .	20
4.1	Comparison of power output between the submerged draft tube condition (SDT) and the non-submerged draft tube condition (NSDT). . . . .	28
4.2	Flow curve of the 3I turbine at different heads. . . . .	29
4.3	Power curve of the 3I turbine at different heads. . . . .	29
4.4	Efficiency curve of the 3I turbine at different heads. . . . .	30
4.5	Efficiency hill curve measured at 4 m, 5.5 m and 7 m inlet head. . . . .	30
4.6	Efficiency hill contour plot. . . . .	31
4.7	Range of Specific Speeds for Various Types of Turbomachinery (Dixon and Hall, 2010). . . . .	32
4.8	Power curve at 5.5 m head. . . . .	33
4.9	Power curve zoomed in on the operation point and the regulation ranges. . . . .	33
5.1	Thermoplastic adhesive between the rotor vanes. . . . .	39
5.2	Curve measurement using a profile gauge. . . . .	39
5.3	Plotting of the curvatures. . . . .	40
5.4	Drawing of the hydro turbine under investigation. . . . .	40
5.5	Physical geometry of the turbine versus the flow field simulation domain. . . . .	41
5.6	2D projection of the hub and shroud contours. . . . .	42
5.7	Project schematics of the simulation of the Indalma turbine. . . . .	43

5.8	Mesh statistics of a single fluid passage in the rotor.	45
5.9	Octree mesh generation.	47
5.10	Delaunay mesh generation.	47
5.11	Tetra/prism mesh generation.	48
6.1	Velocity vector field and pressure distribution of the volute casing.	51
6.2	Simulation results of the rotor region.	52
6.3	Meridional view of the rotor vane.	53
6.4	Blade loading chart.	54
6.5	Vortex field within the turbine rotor.	54
7.1	Flow curves at constant head.	57
7.2	Power curves at constant head.	58
7.3	Efficiency curves at constant head.	58

# List of Tables

2.1	Hydropower plant categories <sup>1</sup>	6
4.1	Measurements at 7 m head with submerged draft tube	25
4.2	Measurements at 5.5 m head with submerged draft tube	26
4.3	Measurements at 4 m head with submerged draft tube	27
4.4	Measurements at 4 m head without submerged draft tube	27
5.1	Experimentally measured data at BEP	37
A.1	First measurements at 7 m head with submerged draft tube	71
A.2	Second measurements at 7 m head with submerged draft tube	71
A.3	First measurements at 7 m head without submerged draft tube	72
A.4	Second measurements at 7 m head without submerged draft tube	72
A.5	First measurements at 5.5 m head with submerged draft tube	72
A.6	Second measurements at 5.5 m head with submerged draft tube	73
A.7	First measurements at 5.5 m head without submerged draft tube	73
A.8	Second measurements at 5.5 m head without submerged draft tube	73
A.9	First measurements at 4 m head with submerged draft tube	74
A.10	Second measurements at 4 m head with submerged draft tube	74
A.11	First measurements at 4 m head without submerged draft tube	74
A.12	Second measurements at 4 m head without submerged draft tube	75



---

## Apendices



# A

## Compilation of accumulated data

	Water Level (m)	Rotational Speed (rpm)	Strain Gauge 1 (RAW)	Strain Gauge 2 (RAW)	Pinlet (RAW)	Manometer Left (m)	Manometer Right (m)	Total Head (m)	Flow Rate (l/s)	Strain Gauge 1 (N)	Strain Gauge 2 (N)	Shaft Torque (Nm)	Shaft Power (W)	Pinlet (cm H <sub>2</sub> O)	Portlet (cm H <sub>2</sub> O)	$\eta_{hydr}$ (%)	$\eta_{mech}$ (%)	$\eta_{tot}$ (%)
	Measured Data									Calculated Data								
0.234	1760	0	0	223.5	0.880	1.365	7.00	11.4	0.0	0.0	0	0	567	48.50	76.0	0.0	0.0	
0.243	1600	0	10	207.8	0.985	1.285	7.01	13.2	0.2	18.4	1	217	528	30.00	72.9	32.8	23.9	
0.253	1300	1	25	178.9	1.115	1.192	7.00	15.5	2.0	45.8	3	423	454	7.70	65.6	60.8	39.9	
0.257	1150	5	36	166.4	1.210	1.130	7.02	16.4	9.3	65.9	4	484	422	-8.00	63.1	67.8	42.8	
0.261	1050	18	55	162.7	1.272	1.094	7.00	17.4	33.0	100.5	5	527	413	-17.80	63.4	69.6	44.1	
0.263	830	21	65	148.9	1.263	1.100	7.03	17.9	38.5	118.8	6	495	378	-16.30	57.9	69.3	40.1	
0.264	580	37	91	141.7	1.260	1.101	7.00	18.2	67.7	166.2	7	425	359	-15.90	55.5	61.4	34.1	
0.265	320	56	116	138.3	1.257	1.104	7.02	18.5	102.4	211.8	8	260	350	-15.30	54.0	38.1	20.5	
0.265	160	67	132	137.9	1.230	1.120	7.02	18.5	122.4	241.0	8	141	349	-11.00	53.2	20.9	11.1	

Table A.1.: First measurements at 7 m head with submerged draft tube.

	Water Level (m)	Rotational Speed (rpm)	Strain Gauge 1 (RAW)	Strain Gauge 2 (RAW)	Pinlet (RAW)	Manometer Left (m)	Manometer Right (m)	Total Head (m)	Flow Rate (l/s)	Strain Gauge 1 (N)	Strain Gauge 2 (N)	Shaft Torque (Nm)	Shaft Power (W)	Pinlet (cm H <sub>2</sub> O)	Portlet (cm H <sub>2</sub> O)	$\eta_{hydr}$ (%)	$\eta_{mech}$ (%)	$\eta_{tot}$ (%)
	Measured Data									Calculated Data								
0.233	1770	0	0	229.3	0.870	1.362	7.01	11.2	0.0	0.0	0	0	582	49.2	77.9	0.0	0.0	
0.247	1480	3	17	197.8	1.050	1.228	7.01	14.1	5.7	31.2	2	281	502	17.8	71.0	40.9	29.0	
0.253	1340	5	27	186.0	1.105	1.192	6.99	15.5	9.3	49.4	3	400	472	8.7	68.2	55.4	37.7	
0.257	1170	10	39	172.2	1.225	1.110	7.02	16.4	18.4	71.3	4	460	437	-11.5	65.7	62.0	40.7	
0.260	980	13	51	159.8	1.275	1.082	7.03	17.2	23.9	93.2	5	505	405	-19.3	62.3	68.6	42.7	
0.263	830	17	61	150.7	1.267	1.087	7.03	17.9	31.2	111.5	6	495	382	-18.0	58.8	68.3	40.1	
0.264	700	24	71	149.4	1.272	1.083	7.02	18.2	44.0	129.7	6	446	379	-18.9	58.5	61.0	35.7	
0.265	590	32	82	146.1	1.266	1.088	7.01	18.5	58.6	149.8	6	400	370	-17.8	57.3	55.2	31.6	
0.265	500	41	94	145.3	1.267	1.086	7.00	18.5	75.0	171.7	7	360	368	-18.1	57.1	49.8	28.4	
0.266	370	51	108	142.8	1.267	1.086	7.01	18.7	93.2	197.2	7	286	362	-18.1	56.1	39.7	22.3	
0.266	190	65	122	140.9	1.253	1.096	7.01	18.7	118.8	222.8	7	147	357	-15.7	55.1	20.8	11.4	

Table A.2.: Second measurements at 7 m head with submerged draft tube.

Water Level (m)	Rotational Speed (rpm)	Strain Gauge 1 (RAW)	Strain Gauge 2 (RAW)	Pinlet (RAW)	Manometer Left (m)	Manometer Right (m)	Total Head (m)	Flow Rate (l/s)	Strain Gauge 1 (N)	Strain Gauge 2 (N)	Shaft Torque (Nm)	Shaft Power (W)	Pinlet (cm H <sub>2</sub> O)	Portlet (cm H <sub>2</sub> O)	$\eta_{hydr}$ (%)	$\eta_{mech}$ (%)	$\eta_{tot}$ (%)
Measured Data									Calculated Data								
0.228	1720	0	0	233.2	0.870	1.380	7.01	10.3	0.0	0.0	0	592	51.00	79.1	0.0	0.0	
0.234	1640	1	6	225.1	0.890	1.365	7.02	11.4	2.0	11.1	1	111	572	47.50	76.5	18.5	14.2
0.243	1420	1	13	207.1	0.917	1.342	7.00	13.2	2.0	23.9	2	231	526	42.50	70.9	35.9	25.5
0.246	1320	1	18	198.5	0.940	1.320	7.01	13.9	2.0	33.0	2	304	504	38.00	68.3	46.7	31.9
0.248	1270	2	22	193.8	0.964	1.305	7.02	14.3	3.8	40.3	3	345	492	34.10	67.1	52.1	35.0
0.253	1180	3	28	181.4	1.025	1.255	7.03	15.5	5.7	51.3	3	400	460	23.00	64.1	58.6	37.6
0.255	1060	9	40	169.9	1.115	1.202	6.99	16.0	16.6	73.2	4	446	431	8.70	62.3	65.5	40.8
0.258	980	13	50	160.3	1.145	1.175	7.00	16.7	23.9	91.4	5	492	406	3.00	59.5	72.3	43.0
0.260	780	20	62	157.8	1.135	1.190	7.02	17.2	36.7	113.3	5	444	400	5.50	58.1	64.8	37.6
0.261	620	27	73	154.6	1.105	1.205	7.03	17.4	49.4	133.4	6	387	392	10.00	56.2	57.4	32.3
0.261	540	38	89	152.2	1.108	1.203	7.03	17.4	69.5	162.6	7	374	386	9.50	55.4	56.2	31.1
0.262	450	43	97	142.8	1.122	1.196	7.03	17.7	78.6	177.2	7	330	362	7.40	52.3	51.8	27.1
0.263	330	52	107	144.4	1.125	1.198	7.02	17.9	95.1	195.4	7	246	366	7.30	53.0	37.7	20.0
0.263	210	60	118	145.1	1.095	1.210	7.03	17.9	109.7	215.5	8	165	368	11.50	52.6	25.5	13.4
0.263	130	64	123	146.2	1.085	1.222	7.00	17.9	117.0	224.6	8	104	371	13.70	52.9	16.0	8.5

**Table A.3.:** First measurements at 7 m head without submerged draft tube.

Water Level (m)	Rotational Speed (rpm)	Strain Gauge 1 (RAW)	Strain Gauge 2 (RAW)	Pinlet (RAW)	Manometer Left (m)	Manometer Right (m)	Total Head (m)	Flow Rate (l/s)	Strain Gauge 1 (N)	Strain Gauge 2 (N)	Shaft Torque (Nm)	Shaft Power (W)	Pinlet (cm H <sub>2</sub> O)	Portlet (cm H <sub>2</sub> O)	$\eta_{hydr}$ (%)	$\eta_{mech}$ (%)	$\eta_{tot}$ (%)
Measured Data									Calculated Data								
0.227	1740	0	0	235.8	0.850	1.370	7.01	10.1	0.0	0.0	0	599	52.00	79.9	0.0	0.0	
0.238	1520	2	11	211.2	0.887	1.336	7.00	12.2	3.8	20.2	1	186	536	44.90	72.1	30.8	22.2
0.245	1340	3	21	197	0.920	1.312	7.00	13.7	5.7	38.5	2	327	500	39.20	67.7	51.6	34.9
0.248	1190	6	31	181.8	0.967	1.273	7.00	14.3	11.1	56.7	3	404	461	30.60	63.4	64.8	41.1
0.254	1070	11	43	172.4	1.087	1.193	7.02	15.7	20.2	78.6	4	465	437	10.60	62.7	68.6	43.0
0.262	950	16	55	158.5	1.115	1.175	7.01	17.7	29.4	100.5	5	503	402	6.00	58.3	71.0	41.4
0.258	740	22	64	154.1	1.107	1.180	7.01	16.7	40.3	117.0	5	422	391	7.30	56.6	65.1	36.8
0.258	570	32	79	153.5	1.082	1.197	7.00	16.7	58.6	144.3	6	363	389	11.50	55.8	56.9	31.8
0.261	370	49	102	147.8	1.100	1.186	7.01	17.4	89.6	186.3	7	266	375	8.60	54.1	41.1	22.2
0.263	200	59	114	150.8	1.080	1.197	7.01	17.9	107.8	208.2	7	149	382	11.70	54.8	22.1	12.1

**Table A.4.:** Second measurements at 7 m head without submerged draft tube.

Water Level (m)	Rotational Speed (rpm)	Strain Gauge 1 (RAW)	Strain Gauge 2 (RAW)	Pinlet (RAW)	Manometer Left (m)	Manometer Right (m)	Total Head (m)	Flow Rate (l/s)	Strain Gauge 1 (N)	Strain Gauge 2 (N)	Shaft Torque (Nm)	Shaft Power (W)	Pinlet (cm H <sub>2</sub> O)	Portlet (cm H <sub>2</sub> O)	$\eta_{hydr}$ (%)	$\eta_{mech}$ (%)	$\eta_{tot}$ (%)
Measured Data									Calculated Data								
0.226	1580	0	0	176.6	0.955	1.295	5.50	9.9	0.0	0.0	0	448	34.00	77.7	0.0	0.0	
0.240	1310	0	12	150.9	1.102	1.195	5.50	12.6	0.2	22.1	2	213	383	9.30	70.3	44.7	31.4
0.247	1140	4	22	138.4	1.165	1.152	5.52	14.1	7.5	40.3	2	278	351	-1.30	66.1	55.2	36.5
0.250	970	6	32	123.8	1.250	1.100	5.49	14.8	11.1	58.6	3	342	314	-15.00	62.3	69.1	43.0
0.253	880	8	38	119.0	1.277	1.082	5.50	15.5	14.8	69.5	4	358	301	-19.50	60.7	70.7	43.0
0.255	680	13	49	113.7	1.275	1.085	5.49	16.0	23.9	89.6	5	332	288	-19.00	58.3	66.4	38.7
0.257	510	20	61	107.2	1.257	1.090	5.49	16.4	36.7	111.5	5	284	271	-16.70	54.8	58.5	32.1
0.257	350	28	72	104.9	1.267	1.088	5.50	16.4	51.3	131.6	6	209	265	-17.90	53.9	43.8	23.6
0.258	170	38	85	105.6	1.253	1.097	5.49	16.7	69.5	155.3	6	108	267	-15.60	53.9	22.4	12.1

**Table A.5.:** First measurements at 5.5 m head with submerged draft tube.

	Water Level (m)	Rotational Speed (rpm)	Strain Gauge 1 (RAW)	Strain Gauge 2 (RAW)	Pinlet (RAW)	Manometer Left (m)	Manometer Right (m)	Total Head (m)	Flow Rate (/s)	Strain Gauge 1 (N)	Strain Gauge 2 (N)	Shaft Torque (Nm)	Shaft Power (W)	Pinlet (cm H <sub>2</sub> O)	Poutlet (cm H <sub>2</sub> O)	$\eta_{hydr}$ (%)	$\eta_{mech}$ (%)	$\eta_{tot}$ (%)
	Measured Data									Calculated Data								
0.227	1580	0	0	174.9	0.955	1.290	5.50	10.1	0.0	0.0	0	444	33.5	77.0	0.0	0.0	0.0	
0.235	1460	7	14	164.3	1.015	1.245	5.50	11.6	12.9	25.7	1	139	417	23.0	74.0	30.0	22.2	
0.243	1270	4	20	147.2	1.118	1.177	5.49	13.2	7.5	36.7	2	276	373	5.9	69.3	55.9	38.7	
0.249	1070	8	31	133.6	1.206	1.125	5.50	14.6	14.8	56.7	3	334	338	-8.1	65.4	65.1	42.6	
0.252	930	10	40	122.0	1.261	1.091	5.50	15.2	18.4	73.2	4	379	309	-17.0	61.7	74.8	46.1	
0.255	830	13	46	116.4	1.270	1.077	5.50	16.0	23.9	84.1	4	372	295	-19.3	59.5	72.7	43.3	
0.256	670	18	55	114.3	1.281	1.076	5.52	16.2	33.0	100.5	5	336	289	-20.5	58.5	65.7	38.4	
0.257	500	25	67	108.0	1.272	1.085	5.50	16.4	45.8	122.4	5	285	273	-18.7	55.5	58.0	32.2	
0.258	350	34	79	106.5	1.272	1.085	5.49	16.7	62.2	144.3	6	214	269	-18.7	54.9	43.4	23.8	
0.258	170	47	94	106.9	1.256	1.094	5.49	16.7	85.9	171.7	6	108	271	-16.2	54.6	22.1	12.1	

Table A.6.: Second measurements at 5.5 m head with submerged draft tube.

	Water Level (m)	Rotational Speed (rpm)	Strain Gauge 1 (RAW)	Strain Gauge 2 (RAW)	Pinlet (RAW)	Manometer Left (m)	Manometer Right (m)	Total Head (m)	Flow Rate (/s)	Strain Gauge 1 (N)	Strain Gauge 2 (N)	Shaft Torque (Nm)	Shaft Power (W)	Pinlet (cm H <sub>2</sub> O)	Poutlet (cm H <sub>2</sub> O)	$\eta_{hydr}$ (%)	$\eta_{mech}$ (%)	$\eta_{tot}$ (%)
	Measured Data									Calculated Data								
0.223	1530	0	0	181.3	0.925	1.325	5.50	9.4	0.0	0.0	0	460	40.00	78.8	0.0	0.0	0.0	
0.240	1190	0	13	155.4	0.977	1.287	5.49	12.6	0.2	23.9	2	210	394	31.00	68.5	45.2	31.0	
0.242	1140	3	19	149.7	0.993	1.277	5.50	13.0	5.7	34.8	2	247	380	28.40	66.3	53.2	35.3	
0.248	950	1	25	130.1	1.114	1.195	5.50	14.3	2.0	45.8	3	309	330	8.10	60.9	65.9	40.1	
0.250	890	2	30	129.8	1.136	1.181	5.50	14.8	3.8	54.9	4	338	329	4.50	61.4	69.2	42.5	
0.253	750	8	38	123.9	1.148	1.174	5.50	15.5	14.8	69.5	4	305	314	2.60	59.0	62.1	36.6	
0.253	700	14	50	123.2	1.135	1.182	5.50	15.5	25.7	91.4	5	342	312	4.70	58.3	70.4	41.0	
0.254	590	19	55	119.9	1.114	1.195	5.51	15.7	34.8	100.5	5	288	304	8.10	56.0	60.7	34.0	
0.253	490	26	65	118.0	1.112	1.195	5.51	15.5	47.6	118.8	5	259	299	8.30	55.1	56.3	31.0	
0.254	390	31	75	115.1	1.124	1.187	5.50	15.7	56.7	137.0	6	233	291	6.30	54.2	50.7	27.5	
0.255	100	42	87	115.0	1.107	1.196	5.51	16.0	76.8	158.9	6	61	291	8.90	53.6	13.2	7.1	
0.255	130	47	93	113.5	1.095	1.208	5.50	16.0	85.9	169.9	6	81	287	11.30	52.6	18.0	9.4	

Table A.7.: First measurements at 5.5 m head without submerged draft tube.

	Water Level (m)	Rotational Speed (rpm)	Strain Gauge 1 (RAW)	Strain Gauge 2 (RAW)	Pinlet (RAW)	Manometer Left (m)	Manometer Right (m)	Total Head (m)	Flow Rate (/s)	Strain Gauge 1 (N)	Strain Gauge 2 (N)	Shaft Torque (Nm)	Shaft Power (W)	Pinlet (cm H <sub>2</sub> O)	Poutlet (cm H <sub>2</sub> O)	$\eta_{hydr}$ (%)	$\eta_{mech}$ (%)	$\eta_{tot}$ (%)
	Measured Data									Calculated Data								
0.222	1540	0	0	181.2	0.912	1.316	5.50	9.2	0.0	0.0	0	460	40.40	78.6	0.0	0.0	0.0	
0.229	1380	3	9	168.1	0.939	1.292	5.50	10.5	5.7	16.6	1	112	426	35.30	73.5	27.2	20.0	
0.238	1180	1	14	151.5	0.968	1.275	5.50	12.2	2.0	25.7	2	208	384	30.70	66.6	47.5	31.7	
0.243	1070	3	22	144.4	0.998	1.251	5.50	13.2	5.7	40.3	2	276	366	25.30	64.3	60.1	38.7	
0.247	1000	6	28	137.0	1.092	1.186	5.52	14.1	11.1	51.3	3	298	347	9.40	63.6	61.5	39.1	
0.249	890	9	37	126.7	1.130	1.163	5.51	14.6	16.6	67.7	4	338	321	3.30	60.1	71.7	43.0	
0.250	670	15	48	120.4	1.124	1.169	5.50	14.8	27.5	87.8	4	300	305	4.50	57.0	66.1	37.7	
0.252	500	21	57	120.9	1.099	1.184	5.50	15.2	38.5	104.2	5	244	306	8.50	56.5	52.6	29.7	
0.255	360	28	69	116.1	1.112	1.175	5.50	16.0	51.3	126.1	5	200	294	6.30	54.7	42.6	23.3	
0.255	140	42	84	113.6	1.075	1.194	5.50	16.0	76.8	153.4	5	80	288	11.90	52.5	17.7	9.3	

Table A.8.: Second measurements at 5.5 m head without submerged draft tube.

Water Level (m)	Rotational Speed (rpm)	Strain Gauge 1 (RAW)	Strain Gauge 2 (RAW)	Pinlet (RAW)	Manometer Left (m)	Manometer Right (m)	Total Head (m)	Flow Rate (l/s)	Strain Gauge 1 (N)	Strain Gauge 2 (N)	Shaft Torque (Nm)	Shaft Power (W)	Pinlet (cm H <sub>2</sub> O)	Poutlet (cm H <sub>2</sub> O)	$\eta_{hydr}$ (%)	$\eta_{mech}$ (%)	$\eta_{tot}$ (%)
Measured Data									Calculated Data								
0.220	1360	0	0	127.1	1.035	1.235	4.00	8.9	0.0	0.0	0	0	322	20.0	78.8	0.0	0.0
0.230	1160	4	12	110.8	1.125	1.175	4.02	10.6	7.5	22.1	1	126	280	5.0	71.8	41.9	30.1
0.240	900	3	20	92.4	1.240	1.105	4.01	12.6	5.7	36.7	2	208	233	-13.5	64.9	64.6	41.9
0.244	790	5	26	86.3	1.278	1.078	4.00	13.5	9.3	47.6	3	225	218	-20.0	62.8	68.0	42.7
0.245	590	9	35	82.3	1.283	1.076	4.02	13.7	16.6	64.0	3	208	208	-20.7	60.1	64.3	38.7
0.247	400	14	45	78.1	1.275	1.081	4.01	14.1	25.7	82.3	4	168	197	-19.4	57.3	53.0	30.4
0.248	210	23	56	72.9	1.270	1.085	4.00	14.3	42.1	102.4	4	94	184	-18.5	53.9	31.1	16.7
0.249	110	28	63	73.7	1.257	1.094	4.00	14.6	51.3	115.1	5	52	186	-16.3	53.9	17.0	9.2

**Table A.9.:** First measurements at 4 m head with submerged draft tube.

Water Level (m)	Rotational Speed (rpm)	Strain Gauge 1 (RAW)	Strain Gauge 2 (RAW)	Pinlet (RAW)	Manometer Left (m)	Manometer Right (m)	Total Head (m)	Flow Rate (l/s)	Strain Gauge 1 (U)	Strain Gauge 2 (N)	Shaft Torque (Nm)	Shaft Power (W)	Pinlet (cm H <sub>2</sub> O)	Poutlet (cm H <sub>2</sub> O)	$\eta_{hydr}$ (%)	$\eta_{mech}$ (%)	$\eta_{tot}$ (%)
Measured Data									Calculated Data								
0.220	1360	0	0	123.4	1.048	1.232	3.99	8.9	0.0	0.0	0	0	312	18.40	77.0	0.0	0.0
0.228	1240	6	11	115.1	1.107	1.189	4.00	10.3	11.1	20.2	1	84	291	8.20	74.1	28.2	20.9
0.237	1030	2	15	100.8	1.182	1.140	4.00	12.0	3.8	27.5	2	182	255	-4.20	68.1	56.8	38.7
0.239	940	4	20	94.9	1.220	1.114	4.01	12.4	7.5	36.7	2	204	240	-10.60	65.8	63.7	41.9
0.244	760	8	31	84.1	1.285	1.075	3.99	13.5	14.8	56.7	3	237	212	-21.00	61.8	73.0	45.1
0.246	600	12	38	77.6	1.284	1.076	4.01	13.9	22.1	69.5	3	212	196	-20.80	57.4	67.7	38.8
0.247	440	17	48	75.8	1.281	1.078	3.99	14.1	31.2	87.8	4	185	191	-20.30	56.4	59.6	33.6
0.248	280	24	58	75.2	1.280	1.076	4.00	14.3	44.0	106.0	4	129	190	-20.40	55.8	41.2	23.0
0.249	100	32	69	75.7	1.263	1.092	4.01	14.6	58.6	126.1	5	50	191	-17.10	55.2	15.9	8.8

**Table A.10.:** Second measurements at 4 m head with submerged draft tube.

Water Level (m)	Rotational Speed (rpm)	Strain Gauge 1 (RAW)	Strain Gauge 2 (RAW)	Pinlet (RAW)	Manometer Left (m)	Manometer Right (m)	Total Head (m)	Flow Rate (l/s)	Strain Gauge 1 (N)	Strain Gauge 2 (N)	Shaft Torque (Nm)	Shaft Power (W)	Pinlet (cm H <sub>2</sub> O)	Poutlet (cm H <sub>2</sub> O)	$\eta_{hydr}$ (%)	$\eta_{mech}$ (%)	$\eta_{tot}$ (%)
Measured Data									Calculated Data								
0.215	1300	0	0	130.0	0.970	1.270	4.00	8.0	0.0	0.0	0	0	329	30.0	78.1	0.0	0.0
0.223	1120	3	8	118.8	0.987	1.256	3.97	9.4	5.7	14.8	1	76	301	26.9	72.3	28.8	20.9
0.233	950	1	14	106.9	1.060	1.198	3.98	11.2	2.0	25.7	2	168	271	13.8	67.8	56.6	38.4
0.238	760	3	21	93.0	1.129	1.164	4.00	12.2	5.7	38.5	2	186	235	3.5	61.2	63.5	38.8
0.240	660	5	26	90.0	1.140	1.156	3.99	12.6	9.3	47.6	3	188	227	1.6	59.9	63.7	38.2
0.242	480	9	36	86.8	1.105	1.180	4.01	13.0	16.6	65.9	3	176	219	7.5	56.1	61.2	34.4
0.243	350	14	42	85.0	1.116	1.172	4.01	13.2	25.7	76.8	4	133	215	5.6	55.4	46.1	25.6
0.243	130	24	54	83.0	1.095	1.184	4.00	13.2	44.0	98.7	4	53	210	8.9	53.5	19.1	10.2

**Table A.11.:** First measurements at 4 m head without submerged draft tube.

Water Level (m)	Rotational Speed (rpm)	Strain Gauge 1 (RAW)	Strain Gauge 2 (RAW)	Pialet (RAW)	Manometer Left (m)	Manometer Right (m)	Total Head (m)	Flow Rate (/s)	Strain Gauge 1 (N)	Strain Gauge 2 (N)	Shaft Torque (Nm)	Shaft Power (W)	Pialet (cm H <sub>2</sub> O)	Poutlet (cm H <sub>2</sub> O)	$\eta_{hydr}$ (%)	$\eta_{mech}$ (%)	$\eta_{tot}$ (%)
Measured Data								Calculated Data									
0.217	1280	0	0	129.8	0.953	1.256	4.00	8.4	0.0	0.0	0	329	30.30	77.9	0.0	0.0	
0.223	1150	3	9	120.5	0.968	1.244	4.00	9.4	5.7	16.6	1	94	305	27.60	72.7	35.1	25.5
0.229	972	1	12	108.6	0.990	1.229	4.01	10.5	2.0	22.1	1	145	275	23.90	65.8	53.7	35.4
0.235	874	0	16	101.0	1.080	1.160	4.00	11.6	0.2	29.4	2	190	255	8.00	65.2	64.1	41.8
0.237	802	0	19	94.3	1.103	1.151	4.00	12.0	0.2	34.8	2	207	238	4.80	61.7	71.3	44.0
0.238	741	2	21	91.8	1.123	1.139	4.00	12.2	3.8	38.5	2	191	232	1.60	60.9	65.6	40.0
0.240	649	5	25	87.6	1.125	1.138	3.99	12.6	9.3	45.8	3	176	221	1.30	58.4	61.2	35.7
0.241	452	13	38	84.3	1.090	1.160	4.00	12.8	23.9	69.5	3	153	213	7.00	54.8	55.7	30.5
0.243	305	23	52	80.1	1.104	1.151	3.99	13.2	42.1	95.1	4	120	202	4.70	52.8	43.9	23.2
0.243	118	34	65	81.7	1.075	1.165	4.01	13.2	62.2	118.8	4	50	206	9.00	52.5	18.2	9.5

**Table A.12.: Second measurements at 4 m head without submerged draft tube.**



# Used scripts and Arduino sketch

## B.1 lerArduino.sh

---

```

#!/bin/bash

# Written by Ramsay Mac Donald (ramsay_macdonald@yahoo.com)
# 16-12-2013
#
# Created to view and/or log data from an arduino board which sends data with the "serial.print" command everytime the
# character "L" is received with "serial.read"

echo "Which port is the Arduino board on?: ttyACMx"                                # Use "ls /dev" in terminal to find
ttyACMx
ttyACM=0
read ttyACM
export ttyACM
echo "Reading from serial $ttyACM:"                                                 # Configures the serial port for the arduino (speed=115200)
stty -F /dev/$ttyACM 115200 cs8 cread clocal
echo "Do you want to log the data? (y/n)"
selection1=0
read selection1
export selection1

if [ $selection1 = y ]; then
    folderName=0
    echo "Name this test sequence: "                                              # Enter a name for the data folder
    read folderName
    export folderName
    export folderName
    mkdir ./$folderName
    gnome-terminal -e ./tail.sh
    gnome-terminal -e ./splitArduinoData.sh

    while true; do
        echo "L" > /dev/$ttyACM                                         # Program Arduino to
        "serial.print" the data if the character "L" is received from the "serial.read"
        grep -v RAMSAY ./${folderName}/completeLogArduino.txt |tail -n 1 > ./${folderName}/arduino.txt      #
        Writes the last data row to "arduino.txt"
        sleep 1
    done
else
    gnome-terminal -e ./tail.sh
    while true; do
        echo "L" > /dev/$ttyACM                                         # Program Arduino to
        "serial.print" the data if the character "L" is received from the "serial.read"
        sleep 1
        # Enter your own sleep value
    done
fi

```

---

## B.2 tail.sh

---

```

#!/bin/bash

# Written by Ramsay Mac Donald
# 23-12-2013
# Created to view the data while logging a complete log in the "completeLogArduino.txt" file (if required to log data), or
# only to view the data sent by the arduino

```

---

```

if [ ${selection1} = y ]; then
    tail -f /dev/ttyACM${ttyACM} | tee -a ./${folderName}/completeLogArduino.txt
else
    tail -f /dev/ttyACM${ttyACM}
fi

```

---

## B.3 splitArduinoData.sh

```

#!/bin/bash

# Written by Ramsay Mac Donald
# 22-10-2013
# Created to make a selective log file. Press "l" and "enter" to log the last data set.

startsign=0

while true; do
    echo "Press l followed by enter for capturing data"
    read startsign

    while [ ${startsign} = 1 ]; do
        echo "Capturing"
        #i = 1 # For a counter
        cut -d " " -f1 ./${folderName}/arduino.txt >> ./${folderName}/Pressure1.txt
        cut -d " " -f2 ./${folderName}/arduino.txt >> ./${folderName}/Pressure2.txt
        cut -d " " -f3 ./${folderName}/arduino.txt >> ./${folderName}/Pressure3.txt
        cut -d " " -f4 ./${folderName}/arduino.txt >> ./${folderName}/Pressure4.txt
        cut -d " " -f4 ./${folderName}/arduino.txt >> ./${folderName}/Flow.txt
        cut -d " " -f6 ./${folderName}/arduino.txt >> ./${folderName}/RPMInterrupt.txt
        cut -d " " -f1-6 ./${folderName}/arduino.txt >> ./${folderName}/plotLog.txt
        #i = $((i + 1)) # count
        startsign=0
        export startsign
    done
done

```

---

## B.4 arduinoScript.ino

```

// Written By Ramsay Mac Donald
// 19-12-2013
// ramsay_macdonald@yahoo.com
// For Arduino UNO

#include <LiquidCrystal.h>

const unsigned int rs = 11;
const unsigned int rw = 10;
const unsigned int d4 = 7;
const unsigned int d5 = 6;
const unsigned int d6 = 5;
const unsigned int d7 = 4;

const int PWMPin = 9;
const int sensorPin = A0;
const int sensorPin1 = A1;
const int sensorPin2 = A2;
const int sensorPin3 = A3;

/*
const float calibrationSlope = 2.5472;           // (a) from the function you get in the calibration graph (y=ax+b) of
                                                 // the 2.5 Bar Pressure transducer
const float calibrationOffset = -1.7877;         // (b) from the function you get in the calibration graph (y=ax+b) of
                                                 // the 2.5 Bar Pressure transducer
*/
float reading = 0.0;
float reading1 = 0.0;
float reading2 = 0.0;
float reading3 = 0.0;

```

```

const unsigned int tempo = 1;
const unsigned int printDlay = 200;
const unsigned int Dlay = printDlay/18;

volatile double Pulse = 0.0;
volatile double flowRate = 0.0;
const float flowRateFactor = 1.0; // the amount of liters that pass the flow sensor per pulse

volatile double Pulse1 = 0.0;
volatile double RPMRate = 0.0;
unsigned int RPMDisplayed = 0;
const float RPMFactor = 60.0; // 60 devided by the amount of pulses per rotation

unsigned char x;

LiquidCrystal lcd(rs, rw, d4, d5, d6, d7);

void setup()
{
    pinMode(PWMPin, OUTPUT);
    Serial.begin(115200);
    Serial.flush();
    lcd.begin(2, 40);
    lcd.clear();
    lcd.home();
    lcd.print("Indalma Testing");
    lcd.setCursor(16, 0);
    lcd.print(" Commencing");
    delay(1000);
    lcd.clear();
    attachInterrupt(0,flowSense,FALLING);
    attachInterrupt(1,RPM,FALLING);
}

void loop() {

//++++++_ANALOG_PIN_A0_(2.5_BAR_PRESSURE_SENSOR)_++++++

reading = variable();
//Serial.print(reading); // print output to serial with interval "printDlay"

x=Serial.read();
if (x=='L')
{
//Serial.print(analogRead(sensorPin)); // use for integer instead of float value
Serial.print(reading);
}
lcd.setCursor(0, 0);
lcd.print(" ");
lcd.setCursor(1, 0);
lcd.print(reading); // analog input pin A0

/*lcd.setCursor(0, 1);
lcd.print(" ");
lcd.setCursor(1, 1);
pressureDifference = analogRead(sensorPin);*/
//pressureDifference = map(pressureDifference, 0, 1023, 0.0, 250.0);
//lcd.print(reading);

//++++++_ANALOG_PIN_A1_++++++

reading1 = variable1();
//Serial.print(" "); // print output to serial with interval "printDlay"
//Serial.println(reading1); // print output to serial with interval "printDlay"

if (x=='L')
{
    Serial.print(" ");
    //Serial.print(analogRead(sensorPin1)); // use for integer instead of float value
    Serial.print(reading1);
}
lcd.setCursor(6, 0);
lcd.print(" ");
lcd.setCursor(6, 0);
lcd.print(reading1); // analog input pin A1

//++++++_ANALOG_PIN_A2_++++++

reading2 = variable2();

```

```

//Serial.print(" ");
//Serial.print(reading2);                                // print output to serial with interval "printDlay"
// print output to serial with interval "printDlay"

if (x=='L')
{
  Serial.print(" ");
  //Serial.print(analogRead(sensorPin2));           // use for integer instead of float value
  Serial.print(reading2);
}

lcd.setCursor(11, 0);
lcd.print(" ");
lcd.setCursor(11, 0);
lcd.print(reading2);                                //analog input pin A2

//*****_ANALOG_PIN_A3_*****

reading3 = variable3();
//Serial.print(" ");
//Serial.println(reading3);                                // print output to serial with interval "printDlay"
// print output to serial with interval "printDlay"

if (x=='L')
{
  Serial.print(" ");
  //Serial.print(analogRead(sensorPin3));           // use for integer instead of float value
  Serial.print(reading3);
}

lcd.setCursor(16, 0);
lcd.print(" ");
lcd.setCursor(16, 0);
lcd.print(reading3);                                // analog input pin A3

//*****_FLOW_SENSOR_*****

if (x=='L')
{
  Serial.print(" ");
  //Serial.print(analogRead(flowRate));           // use for integer instead of float value
  Serial.print(flowRate);
}

lcd.setCursor(21, 0);
lcd.print(" ");
lcd.setCursor(21, 0);
lcd.print(flowRate);                                // flowrate sensor

//*****_RPM_SENSOR_*****

RPMDisplayed=RPMrate;
if (x=='L')
{
  Serial.print(" ");
  //Serial.print(analogRead(flowRate));           // use for integer instead of float value
  Serial.println(RPMDisplayed);
}

lcd.setCursor(26, 0);
lcd.print(" ");
lcd.setCursor(26, 0);
lcd.print(RPMDisplayed);                            // flowrate sensor

//*****_FUNCTIONS_*****

//analogWrite(PWMPin, 0);
//delay(100);
analogWrite(PWMPin, 1023);
//delay(100);
//analogWrite(PWMPin, 512);
//delay(100);
//analogWrite(PWMPin, 1023);
//delay(100);
//analogWrite(PWMPin, 512);
//delay(100);
//analogWrite(PWMPin, 255);
//delay(100);
//analogWrite(PWMPin, 0);
Serial.flush();
delay(printDlay);
}

float variable(){                                // used for analog input Pin A0 (1 bar pressure sensor)
  float value[Dlay/tempo];
  float meanValue = 0.00;
  float anaVal = 0.00;
}

```

```

for (int i=0; i<(Dlaly/tempo); i++){
    anaVal = analogRead(sensorPin);
    //anaVal = ((anaVal*calibrationSlope)+calibrationOffset);
    //anaVal = map(anaVal, 0, 1023, 0.00, 1023*calibrationSlope);
    value[i] = anaVal;
    delay(tempo);
}
float sum=0.00;
for (int j=0; j<(Dlaly/tempo); j++){
    sum = sum + value[j];
}
meanValue = (sum/(Dlaly/tempo));
return meanValue;
}

float variable1(){                                // used for analog input Pin A1
float value[Dlaly/tempo];
float meanValue = 0.00;
float anaVal = 0.00;
for (int i=0; i<(Dlaly/tempo); i++){
    anaVal = analogRead(sensorPin1);
    //anaVal = map(anaVal, 0, 1023, 0.00, 5.00);
    value[i] = anaVal;
    delay(tempo);
}
float sum=0.00;
for (int j=0; j<(Dlaly/tempo); j++){
    sum = sum + value[j];
}
meanValue = (sum/(Dlaly/tempo));
return meanValue;
}

float variable2(){                                // used for analog input Pin A2
float value[Dlaly/tempo];
float meanValue = 0.00;
float anaVal = 0.00;
for (int i=0; i<(Dlaly/tempo); i++){
    anaVal = analogRead(sensorPin2);
    //anaVal = map(anaVal, 0, 1023, 0.00, 5.00);
    value[i] = anaVal;
    delay(tempo);
}
float sum=0.00;
for (int j=0; j<(Dlaly/tempo); j++){
    sum = sum + value[j];
}
meanValue = (sum/(Dlaly/tempo));
return meanValue;
}

float variable3(){                                // used for analog input Pin A3
float value[Dlaly/tempo];
float meanValue = 0.00;
float anaVal = 0.00;
for (int i=0; i<(Dlaly/tempo); i++){
    anaVal = analogRead(sensorPin3);
    //anaVal = map(anaVal, 0, 1023, 0.00, 5.00);
    value[i] = anaVal;
    delay(tempo);
}
float sum=0.00;
for (int j=0; j<(Dlaly/tempo); j++){
    sum = sum + value[j];
}
meanValue = (sum/(Dlaly/tempo));
return meanValue;
}

//*****_INTERRUPTS_*****
void flowSense()
{
    volatile double cPulse = micros();
    flowRate = flowRateFactor*(1000000/(cPulse-Pulse));
    Pulse = cPulse;
}

void RPM()
{
    volatile double cPulse1 = micros();

```

```
RPMrate = RPMFactor*(1000000/(cPulse1-Pulse1));  
Pulse1 = cPulse1;  
}
```

---

# ANSYS CFX Report

C

## Section C ANSYS CFX Report

# Simulation Report

## Contents

- [1. File Report](#)  
[Table 1 File Information for CFX](#)
- [2. Mesh Report](#)  
[Table 2 Mesh Information for CFX](#)
- [3. Physics Report](#)  
[Table 3 Domain Physics for CFX](#)  
[Table 4 Boundary Physics for CFX](#)
- [4. Solution Report](#)  
[Table 5 Boundary Flows for CFX](#)
- [5. User Data](#)  
[Chart 1](#)  
[Chart 2](#)  
[Chart 3](#)

## 1. File Report

Table 1. File Information for CFX

Case	CFX
File Path	C:\Users\WB01\Desktop\Simulation Indalma Turbine
File Date	7-May-14
File Time	7:05:30 PM
File Type	CFX5
File Version	15

## 2. Mesh Report

Table 2. Mesh Information for CFX

Domain	Nodes	Elements
File Data1	2966700	2791500
File Data2	470618	1445836
Outlet	62812	230081
All Domains	3500130	4467417

## 3. Physics Report

Table 3. Domain Physics for CFX

Domain - File Data1	
Type	Fluid
Location	Entire Passage
Materials	
Water	
Fluid Definition	Material Library
Morphology	Continuous Fluid
Settings	
Buoyancy Model	Non Buoyant
Domain Motion	Rotating
Alternate Rotation Model	TRUE
Angular Velocity	9.3000e+02 [rev min^-1]
Axis Definition	Coordinate Axis
Rotation Axis	Coord 0.3
Reference Pressure	1.0000e+00 [atm]
Turbulence Model	SST
Turbulent Wall Functions	Automatic
Domain - File Data2	
Type	Fluid
Location	Assembly 2
Materials	
Water	
Fluid Definition	Material Library

Morphology	Continuous Fluid
<i>Settings</i>	
Buoyancy Model	Non Buoyant
Domain Motion	Stationary
Reference Pressure	1.0000e+00 [atm]
Turbulence Model	SST
Turbulent Wall Functions	Automatic
<b>Domain - Outlet</b>	
Type	Fluid
Location	BODY
<i>Materials</i>	
Water	
Fluid Definition	Material Library
Morphology	Continuous Fluid
<i>Settings</i>	
Buoyancy Model	Non Buoyant
Domain Motion	Stationary
Reference Pressure	1.0000e+00 [atm]
Turbulence Model	SST
Turbulent Wall Functions	Automatic
<b>Domain Interface - File Data1 to File Data1 Internal</b>	
Boundary List1	File Data1 to File Data1 Internal Side 1
Boundary List2	File Data1 to File Data1 Internal Side 2
Interface Type	Fluid Fluid
<i>Settings</i>	
Interface Models	General Connection
Mass And Momentum	Conservative Interface Flux
Mesh Connection	GGI
<b>Domain Interface - File Data1 to File Data1 Internal 10</b>	
Boundary List1	File Data1 to File Data1 Internal 10 Side 1
Boundary List2	File Data1 to File Data1 Internal 10 Side 2
Interface Type	Fluid Fluid
<i>Settings</i>	
Interface Models	General Connection
Mass And Momentum	Conservative Interface Flux
Mesh Connection	GGI
<b>Domain Interface - File Data1 to File Data1 Internal 11</b>	
Boundary List1	File Data1 to File Data1 Internal 11 Side 1
Boundary List2	File Data1 to File Data1 Internal 11 Side 2
Interface Type	Fluid Fluid
<i>Settings</i>	
Interface Models	General Connection
Mass And Momentum	Conservative Interface Flux
Mesh Connection	GGI
<b>Domain Interface - File Data1 to File Data1 Internal 12</b>	
Boundary List1	File Data1 to File Data1 Internal 12 Side 1
Boundary List2	File Data1 to File Data1 Internal 12 Side 2
Interface Type	Fluid Fluid
<i>Settings</i>	
Interface Models	General Connection
Mass And Momentum	Conservative Interface Flux
Mesh Connection	GGI
<b>Domain Interface - File Data1 to File Data1 Internal 2</b>	
Boundary List1	File Data1 to File Data1 Internal 2 Side 1
Boundary List2	File Data1 to File Data1 Internal 2 Side 2
Interface Type	Fluid Fluid
<i>Settings</i>	
Interface Models	General Connection
Mass And Momentum	Conservative Interface Flux
Mesh Connection	GGI
<b>Domain Interface - File Data1 to File Data1 Internal 3</b>	
Boundary List1	File Data1 to File Data1 Internal 3 Side 1
Boundary List2	File Data1 to File Data1 Internal 3 Side 2
Interface Type	Fluid Fluid
<i>Settings</i>	
Interface Models	General Connection
Mass And Momentum	Conservative Interface Flux

### Section C ANSYS CFX Report

Mesh Connection	GGI
<b>Domain Interface - File Data1 to File Data1 Internal 4</b>	
Boundary List1	File Data1 to File Data1 Internal 4 Side 1
Boundary List2	File Data1 to File Data1 Internal 4 Side 2
Interface Type	Fluid Fluid
<i>Settings</i>	
Interface Models	General Connection
Mass And Momentum	Conservative Interface Flux
Mesh Connection	GGI
<b>Domain Interface - File Data1 to File Data1 Internal 5</b>	
Boundary List1	File Data1 to File Data1 Internal 5 Side 1
Boundary List2	File Data1 to File Data1 Internal 5 Side 2
Interface Type	Fluid Fluid
<i>Settings</i>	
Interface Models	General Connection
Mass And Momentum	Conservative Interface Flux
Mesh Connection	GGI
<b>Domain Interface - File Data1 to File Data1 Internal 6</b>	
Boundary List1	File Data1 to File Data1 Internal 6 Side 1
Boundary List2	File Data1 to File Data1 Internal 6 Side 2
Interface Type	Fluid Fluid
<i>Settings</i>	
Interface Models	General Connection
Mass And Momentum	Conservative Interface Flux
Mesh Connection	GGI
<b>Domain Interface - File Data1 to File Data1 Internal 7</b>	
Boundary List1	File Data1 to File Data1 Internal 7 Side 1
Boundary List2	File Data1 to File Data1 Internal 7 Side 2
Interface Type	Fluid Fluid
<i>Settings</i>	
Interface Models	General Connection
Mass And Momentum	Conservative Interface Flux
Mesh Connection	GGI
<b>Domain Interface - File Data1 to File Data1 Internal 8</b>	
Boundary List1	File Data1 to File Data1 Internal 8 Side 1
Boundary List2	File Data1 to File Data1 Internal 8 Side 2
Interface Type	Fluid Fluid
<i>Settings</i>	
Interface Models	General Connection
Mass And Momentum	Conservative Interface Flux
Mesh Connection	GGI
<b>Domain Interface - File Data1 to File Data1 Internal 9</b>	
Boundary List1	File Data1 to File Data1 Internal 9 Side 1
Boundary List2	File Data1 to File Data1 Internal 9 Side 2
Interface Type	Fluid Fluid
<i>Settings</i>	
Interface Models	General Connection
Mass And Momentum	Conservative Interface Flux
Mesh Connection	GGI
<b>Domain Interface - File Data1 to File Data2</b>	
Boundary List1	File Data1 to File Data2 Side 1
Boundary List2	File Data1 to File Data2 Side 2
Interface Type	Fluid Fluid
<i>Settings</i>	
Interface Models	General Connection
Frame Change	Stage
Downstream Velocity Constraint	Stage Average Velocity
Pitch Change	Automatic
Mesh Connection	GGI
<b>Domain Interface - Outlet to File Data1</b>	
Boundary List1	Outlet to File Data1 Side 1 1
Boundary List2	Outlet to File Data1 Side 1
Interface Type	Fluid Fluid
<i>Settings</i>	
Interface Models	General Connection
Frame Change	Stage
Downstream Velocity Constraint	Stage Average Velocity

Pitch Change	Automatic
Mesh Connection	GGI

Table 4. Boundary Physics for CFX

Domain	Boundaries	
File Data1		Boundary - File Data1 to File Data1 Internal 10 Side 1
Type		INTERFACE
Location		SHROUD TIP GGI SIDE 1 7
	<i>Settings</i>	
Mass And Momentum		Conservative Interface Flux
Turbulence		Conservative Interface Flux
	Boundary - File Data1 to File Data1 Internal 10 Side 2	
Type		INTERFACE
Location		SHROUD TIP GGI SIDE 2 7
	<i>Settings</i>	
Mass And Momentum		Conservative Interface Flux
Turbulence		Conservative Interface Flux
	Boundary - File Data1 to File Data1 Internal 11 Side 1	
Type		INTERFACE
Location		SHROUD TIP GGI SIDE 1 8
	<i>Settings</i>	
Mass And Momentum		Conservative Interface Flux
Turbulence		Conservative Interface Flux
	Boundary - File Data1 to File Data1 Internal 11 Side 2	
Type		INTERFACE
Location		SHROUD TIP GGI SIDE 2 8
	<i>Settings</i>	
Mass And Momentum		Conservative Interface Flux
Turbulence		Conservative Interface Flux
	Boundary - File Data1 to File Data1 Internal 12 Side 1	
Type		INTERFACE
Location		SHROUD TIP GGI SIDE 1 9
	<i>Settings</i>	
Mass And Momentum		Conservative Interface Flux
Turbulence		Conservative Interface Flux
	Boundary - File Data1 to File Data1 Internal 12 Side 2	
Type		INTERFACE
Location		SHROUD TIP GGI SIDE 2 9
	<i>Settings</i>	
Mass And Momentum		Conservative Interface Flux
Turbulence		Conservative Interface Flux
	Boundary - File Data1 to File Data1 Internal 2 Side 1	
Type		INTERFACE
Location		SHROUD TIP GGI SIDE 1 10
	<i>Settings</i>	
Mass And Momentum		Conservative Interface Flux
Turbulence		Conservative Interface Flux
	Boundary - File Data1 to File Data1 Internal 2 Side 2	
Type		INTERFACE
Location		SHROUD TIP GGI SIDE 2 10
	<i>Settings</i>	
Mass And Momentum		Conservative Interface Flux
Turbulence		Conservative Interface Flux
	Boundary - File Data1 to File Data1 Internal 3 Side 1	
Type		INTERFACE
Location		SHROUD TIP GGI SIDE 1 11
	<i>Settings</i>	
Mass And Momentum		Conservative Interface Flux
Turbulence		Conservative Interface Flux
	Boundary - File Data1 to File Data1 Internal 3 Side 2	
Type		INTERFACE
Location		SHROUD TIP GGI SIDE 2 11
	<i>Settings</i>	
Mass And Momentum		Conservative Interface Flux
Turbulence		Conservative Interface Flux
	Boundary - File Data1 to File Data1 Internal 4 Side 1	

## Section C ANSYS CFX Report

Type	INTERFACE
Location	SHROUD TIP GGI SIDE 1 12
<i>Settings</i>	
Mass And Momentum	Conservative Interface Flux
Turbulence	Conservative Interface Flux
<b>Boundary - File Data1 to File Data1 Internal 4 Side 2</b>	
Type	INTERFACE
Location	SHROUD TIP GGI SIDE 2 12
<i>Settings</i>	
Mass And Momentum	Conservative Interface Flux
Turbulence	Conservative Interface Flux
<b>Boundary - File Data1 to File Data1 Internal 5 Side 1</b>	
Type	INTERFACE
Location	SHROUD TIP GGI SIDE 1 2
<i>Settings</i>	
Mass And Momentum	Conservative Interface Flux
Turbulence	Conservative Interface Flux
<b>Boundary - File Data1 to File Data1 Internal 5 Side 2</b>	
Type	INTERFACE
Location	SHROUD TIP GGI SIDE 2 2
<i>Settings</i>	
Mass And Momentum	Conservative Interface Flux
Turbulence	Conservative Interface Flux
<b>Boundary - File Data1 to File Data1 Internal 6 Side 1</b>	
Type	INTERFACE
Location	SHROUD TIP GGI SIDE 1 3
<i>Settings</i>	
Mass And Momentum	Conservative Interface Flux
Turbulence	Conservative Interface Flux
<b>Boundary - File Data1 to File Data1 Internal 6 Side 2</b>	
Type	INTERFACE
Location	SHROUD TIP GGI SIDE 2 3
<i>Settings</i>	
Mass And Momentum	Conservative Interface Flux
Turbulence	Conservative Interface Flux
<b>Boundary - File Data1 to File Data1 Internal 7 Side 1</b>	
Type	INTERFACE
Location	SHROUD TIP GGI SIDE 1 4
<i>Settings</i>	
Mass And Momentum	Conservative Interface Flux
Turbulence	Conservative Interface Flux
<b>Boundary - File Data1 to File Data1 Internal 7 Side 2</b>	
Type	INTERFACE
Location	SHROUD TIP GGI SIDE 2 4
<i>Settings</i>	
Mass And Momentum	Conservative Interface Flux
Turbulence	Conservative Interface Flux
<b>Boundary - File Data1 to File Data1 Internal 8 Side 1</b>	
Type	INTERFACE
Location	SHROUD TIP GGI SIDE 1 5
<i>Settings</i>	
Mass And Momentum	Conservative Interface Flux
Turbulence	Conservative Interface Flux
<b>Boundary - File Data1 to File Data1 Internal 8 Side 2</b>	
Type	INTERFACE
Location	SHROUD TIP GGI SIDE 2 5
<i>Settings</i>	
Mass And Momentum	Conservative Interface Flux
Turbulence	Conservative Interface Flux
<b>Boundary - File Data1 to File Data1 Internal 9 Side 1</b>	
Type	INTERFACE
Location	SHROUD TIP GGI SIDE 1 6
<i>Settings</i>	
Mass And Momentum	Conservative Interface Flux
Turbulence	Conservative Interface Flux
<b>Boundary - File Data1 to File Data1 Internal 9 Side 2</b>	
Type	INTERFACE

Location	SHROUD TIP GGI SIDE 2 6
<i>Settings</i>	
Mass And Momentum	Conservative Interface Flux
Turbulence	Conservative Interface Flux
<b>Boundary - File Data1 to File Data1 Internal Side 1</b>	
Type	INTERFACE
Location	SHROUD TIP GGI SIDE 1
<i>Settings</i>	
Mass And Momentum	Conservative Interface Flux
Turbulence	Conservative Interface Flux
<b>Boundary - File Data1 to File Data1 Internal Side 2</b>	
Type	INTERFACE
Location	SHROUD TIP GGI SIDE 2
<i>Settings</i>	
Mass And Momentum	Conservative Interface Flux
Turbulence	Conservative Interface Flux
<b>Boundary - File Data1 to File Data2 Side 2</b>	
Type	INTERFACE
Location	Entire Passage INFLOW
<i>Settings</i>	
Mass And Momentum	Conservative Interface Flux
Turbulence	Conservative Interface Flux
<b>Boundary - Outlet to File Data1 Side 1 1</b>	
Type	INTERFACE
Location	Entire OUTBlock OUTFLOW
<i>Settings</i>	
Mass And Momentum	Conservative Interface Flux
Turbulence	Conservative Interface Flux
<b>Boundary - File Data1 Blade</b>	
Type	WALL
Location	BLADE 10, BLADE 11, BLADE 12, BLADE 2, BLADE 3, BLADE 4, BLADE 5, BLADE 6, BLADE 7, BLADE 8, BLADE 9
<i>Settings</i>	
Mass And Momentum	No Slip Wall
Wall Roughness	Smooth Wall
<b>Boundary - File Data1 Default</b>	
Type	WALL
Location	BLD HIGH, BLD LE, BLD LOW, BLD SHROUD TIP, BLD TE
<i>Settings</i>	
Mass And Momentum	No Slip Wall
Wall Roughness	Smooth Wall
<b>Boundary - File Data1 Hub</b>	
Type	WALL
Location	OUTBlock HUB, OUTBlock HUB 10, OUTBlock HUB 11, OUTBlock HUB 12, OUTBlock HUB 2, OUTBlock HUB 3, OUTBlock HUB 4, OUTBlock HUB 5, OUTBlock HUB 6, OUTBlock HUB 7, OUTBlock HUB 8, OUTBlock HUB 9, Passage HUB, Passage HUB 10, Passage HUB 11, Passage HUB 12, Passage HUB 2, Passage HUB 3, Passage HUB 4, Passage HUB 5, Passage HUB 6, Passage HUB 7, Passage HUB 8, Passage HUB 9
<i>Settings</i>	
Mass And Momentum	No Slip Wall
Wall Roughness	Smooth Wall
<b>Boundary - File Data1 Shroud</b>	
Type	WALL
Location	OUTBlock SHROUD, OUTBlock SHROUD 10, OUTBlock SHROUD 11, OUTBlock SHROUD 12, OUTBlock SHROUD 2, OUTBlock SHROUD 3, OUTBlock SHROUD 4, OUTBlock SHROUD 5, OUTBlock SHROUD 6, OUTBlock SHROUD 7, OUTBlock SHROUD 8, OUTBlock SHROUD 9, Passage SHROUD, Passage SHROUD 10, Passage SHROUD 11, Passage SHROUD 12, Passage SHROUD 2, Passage SHROUD 3, Passage SHROUD 4, Passage SHROUD 5, Passage SHROUD 6, Passage SHROUD 7, Passage SHROUD 8, Passage SHROUD 9
<i>Settings</i>	
Mass And Momentum	No Slip Wall
Wall Velocity	Counter Rotating Wall
Wall Roughness	Smooth Wall
File Data2	<b>Boundary - Boundary 1</b>

### Section C ANSYS CFX Report

Type	INLET	
Location	INLET	
<i>Settings</i>		
Flow Direction	Normal to Boundary Condition	
Flow Regime	Subsonic	
Mass And Momentum	Mass Flow Rate	
Mass Flow Rate	1.5280e+01 [kg s^-1]	
Turbulence	Medium Intensity and Eddy Viscosity Ratio	
<b>Boundary - File Data1 to File Data2 Side 1</b>		
Type	INTERFACE	
Location	OUTLET	
<i>Settings</i>		
Mass And Momentum	Conservative Interface Flux	
Turbulence	Conservative Interface Flux	
<b>Boundary - Boundary 2</b>		
Type	WALL	
Location	TURBINE_WALL	
<i>Settings</i>		
Mass And Momentum	No Slip Wall	
Wall Roughness	Smooth Wall	
Outlet	<b>Boundary - Outlet to File Data1 Side 1</b>	
	Type	INTERFACE
	Location	INLET 2
	<i>Settings</i>	
	Mass And Momentum	Conservative Interface Flux
	Turbulence	Conservative Interface Flux
	<b>Boundary - Outlet Outlet</b>	
	Type	OUTLET
	Location	OUTLET 2
	<i>Settings</i>	
	Flow Regime	Subsonic
	Mass And Momentum	Average Static Pressure
	Pressure Profile Blend	5.00E-02
	Relative Pressure	9.9658e+04 [Pa]
	Pressure Averaging	Average Over Whole Outlet
	<b>Boundary - Outlet Wall</b>	
	Type	WALL
	Location	OUTLET_WALL
	<i>Settings</i>	
	Mass And Momentum	No Slip Wall
	Wall Roughness	Smooth Wall

## 4. Solution Report

Table 5. Boundary Flows for CFX

Location	Type	Mass Flow	Momentum		
			X	Y	Z
Boundary 1 ( File Data2 )	Boundary	1.53E+01	1.20E+03	2.94E-06	-8.21E-06
Boundary 2 ( File Data2 )	Boundary	0.00E+00	-1.22E+03	-7.95E+00	1.69E+00
File Data1 Blade ( File Data1 )	Boundary	0.00E+00	-1.16E+01	-1.02E+01	-9.34E+01
File Data1 Default ( File Data1 )	Boundary	0.00E+00	1.13E+01	1.03E+01	-8.15E+00
File Data1 Hub ( File Data1 )	Boundary	0.00E+00	-3.83E-01	-5.55E-01	-1.47E+03
File Data1 Shroud ( File Data1 )	Boundary	0.00E+00	-1.57E-01	1.85E+00	7.36E+02
File Data1 to File Data1 Internal 10 Side 1 ( File Data1 )	Boundary	0.00E+00	0.00E+00	0.00E+00	0.00E+00
File Data1 to File Data1 Internal 10 Side 2 ( File Data1 )	Boundary	0.00E+00	0.00E+00	0.00E+00	0.00E+00
File Data1 to File Data1 Internal 11 Side 1 ( File Data1 )	Boundary	0.00E+00	0.00E+00	0.00E+00	0.00E+00
File Data1 to File Data1 Internal 11 Side 2 ( File Data1 )	Boundary	0.00E+00	0.00E+00	0.00E+00	0.00E+00
File Data1 to File Data1 Internal 12 Side 1 ( File Data1 )	Boundary	0.00E+00	0.00E+00	0.00E+00	0.00E+00
File Data1 to File Data1 Internal 12 Side 2 ( File Data1 )	Boundary	0.00E+00	0.00E+00	0.00E+00	0.00E+00
File Data1 to File Data1 Internal 2 Side 1 ( File Data1 )	Boundary	0.00E+00	0.00E+00	0.00E+00	0.00E+00
File Data1 to File Data1 Internal 2 Side 2 ( File Data1 )	Boundary	0.00E+00	0.00E+00	0.00E+00	0.00E+00
File Data1 to File Data1 Internal 3 Side 1 ( File Data1 )	Boundary	0.00E+00	0.00E+00	0.00E+00	0.00E+00
File Data1 to File Data1 Internal 3 Side 2 ( File Data1 )	Boundary	0.00E+00	0.00E+00	0.00E+00	0.00E+00
File Data1 to File Data1 Internal 4 Side 1 ( File Data1 )	Boundary	0.00E+00	0.00E+00	0.00E+00	0.00E+00
File Data1 to File Data1 Internal 4 Side 2 ( File Data1 )	Boundary	0.00E+00	0.00E+00	0.00E+00	0.00E+00
File Data1 to File Data1 Internal 5 Side 1 ( File Data1 )	Boundary	0.00E+00	0.00E+00	0.00E+00	0.00E+00

File Data1 to File Data1 Internal 5 Side 2 ( File Data1 )	Boundary	0.00E+00	0.00E+00	0.00E+00	0.00E+00
File Data1 to File Data1 Internal 6 Side 1 ( File Data1 )	Boundary	0.00E+00	0.00E+00	0.00E+00	0.00E+00
File Data1 to File Data1 Internal 6 Side 2 ( File Data1 )	Boundary	0.00E+00	0.00E+00	0.00E+00	0.00E+00
File Data1 to File Data1 Internal 7 Side 1 ( File Data1 )	Boundary	0.00E+00	0.00E+00	0.00E+00	0.00E+00
File Data1 to File Data1 Internal 7 Side 2 ( File Data1 )	Boundary	0.00E+00	0.00E+00	0.00E+00	0.00E+00
File Data1 to File Data1 Internal 8 Side 1 ( File Data1 )	Boundary	0.00E+00	0.00E+00	0.00E+00	0.00E+00
File Data1 to File Data1 Internal 8 Side 2 ( File Data1 )	Boundary	0.00E+00	0.00E+00	0.00E+00	0.00E+00
File Data1 to File Data1 Internal 9 Side 1 ( File Data1 )	Boundary	0.00E+00	0.00E+00	0.00E+00	0.00E+00
File Data1 to File Data1 Internal 9 Side 2 ( File Data1 )	Boundary	0.00E+00	0.00E+00	0.00E+00	0.00E+00
File Data1 to File Data1 Internal Side 1 ( File Data1 )	Boundary	0.00E+00	0.00E+00	0.00E+00	0.00E+00
File Data1 to File Data1 Internal Side 2 ( File Data1 )	Boundary	0.00E+00	0.00E+00	0.00E+00	0.00E+00
File Data1 to File Data2 Side 1 ( File Data2 )	Boundary	0.00E+00	0.00E+00	0.00E+00	0.00E+00
File Data1 to File Data2 Side 2 ( File Data1 )	Boundary	0.00E+00	0.00E+00	0.00E+00	0.00E+00
Outlet Outlet ( Outlet )	Boundary	-1.61E+01	-2.02E-01	-5.10E-02	8.76E+02
Outlet Wall ( Outlet )	Boundary	0.00E+00	9.21E-02	-1.59E-01	1.73E+00
Outlet to File Data1 Side 1 1 ( File Data1 )	Boundary	0.00E+00	2.55E-04	3.16E-04	7.79E+00
Outlet to File Data1 Side 1 ( Outlet )	Boundary	0.00E+00	1.78E-04	-3.74E-03	-2.78E+02

## 5. User Data

Chart 1.

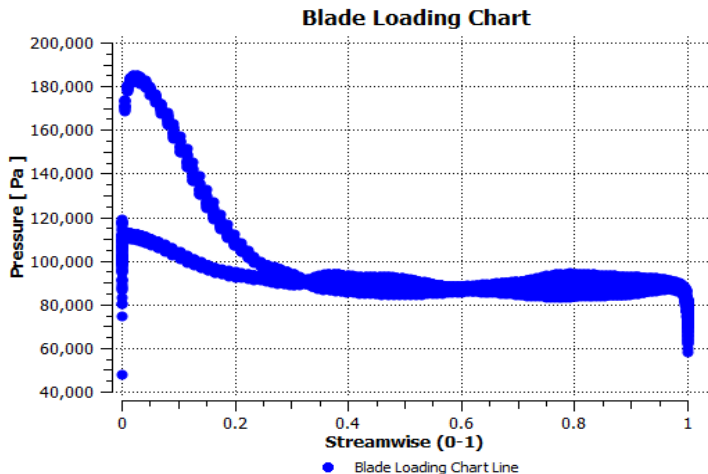
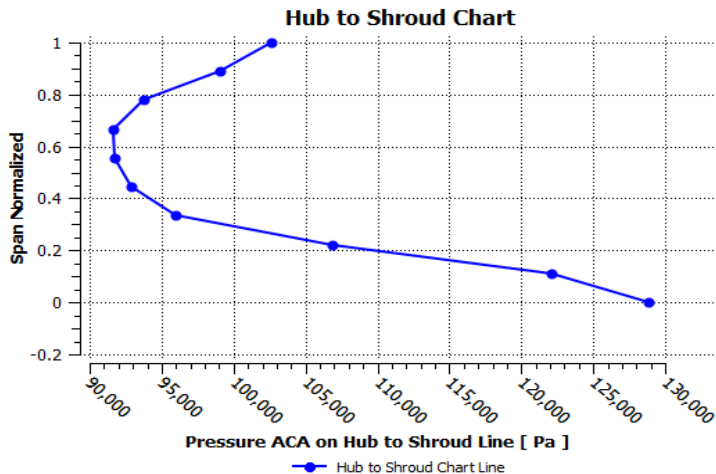


Chart 2.



**Section C ANSYS CFX Report**

Chart 3.

